MYB activity drives emergent enhancer activation and enhancer-promoter interactions in acute lymphoblastic leukemia

Short title: MYB drives enhancer-promoter contact in leukemia

I-Jun Lau[1, 2, 3], Gianna Bloye[1], Alastair L. Smith[1], Joe R. Harman[1, 4], Joseph C. Hamley[1], Vassilena Sharlandjieva[1], Nicholas Denny[1], Catherine Chahrour[1], Hangpeng Li[1], Nicole E. Jackson[1], Paresh Vyas[1, 3], James O.J. Davies[1, 5], Jim R. Hughes[1], Nicholas T. Crump*[6], Thomas A. Milne*[1, 4]

[1] MRC Molecular Haematology Unit, MRC Weatherall Institute of Molecular Medicine, Radcliffe Department of Medicine, University of Oxford, Oxford, UK

[2] Oxford Translational Myeloma Centre (OTMC), Nuffield Department of Orthopaedics, Rheumatology and Musculoskeletal Sciences, University of Oxford, Oxford, UK

[3] Department of Haematology, Oxford University Hospitals NHS Trust, Oxford, UK

[4] Dark Blue Therapeutics Ltd, Oxford, UK

[5] Oxford National Institute of Health Research Biomedical Research Centre, University of Oxford, Oxford, UK

[6] Hugh and Josseline Langmuir Centre for Myeloma Research, Centre for Haematology, Department of Immunology and Inflammation, Imperial College London, London, UK

*Corresponding authors. Email: thomas.milne@imm.ox.ac.uk (TAM), n.crump@imperial.ac.uk (NTC)

Abstract: 218 words

Main text (Intro, Methods, Results, Discussion): 3991 words

Figures: 6, Tables: 0

Supplemental Figures: 11, Supplemental Tables: 4

References: 54

Data Sharing Statement

All high throughput sequencing data have been deposited in the Gene Expression Omnibus (GEO) under accession number GSE296242. The following secure token has been created to alow reviewer access: wzsxoyysjxmbfmb

Key Points

- MYB binding is sufficient to generate enhancers de novo, including formation of enhancer-promoter contacts
- MYB loss in acute lymphoblastic leukemia cells downregulates key oncogenes, with loss of enhancer-promoter contacts

Abstract

Aberrant enhancer usage is a defining feature of oncogenic transcriptional reprogramming. Therapeutic strategies that disrupt enhancer-driven gene regulation may offer new treatment avenues. MYB is a key hematopoietic transcription factor that is frequently dysregulated in a broad range of cancers and plays a critical role in sustaining malignant cell states, including in aggressive leukemia subtypes such as *KMT2A*-rearranged (*KMT2A*-r) leukemias. The molecular mechanisms by which it maintains oncogenic transcription remain incompletely understood. Here, we investigate the role of MYB in directing pathological enhancer activity to drive oncogene expression in leukemia. Using high-resolution Micro-Capture-C, we show that upon MYB degradation, highly defined enhancer-promoter interactions at MYB binding sites are lost, correlating with significant downregulation of target gene expression. When anchored to a gene desert region, the Myb transactivation domain (Myb^{TA}) is sufficient and necessary for nucleation of an enhancer-like region. Critically, long-range chromatin interactions are established up to 400 kb away from where Myb^{TA} is anchored. This results in the activation of transcription from distal cryptic elements, which is reduced or abolished in the presence of point mutations that disrupt its interaction with the co-activators P300/CBP. Together, these results indicate that MYB activity alone is sufficient to generate an enhancer, inducing transcription through precise enhancer-promoter crosstalk, and identify the MYB-P300/CBP axis as a therapeutically actionable vulnerability in enhancer-driven malignancies.

Introduction

Reprogramming of enhancer landscapes underlies oncogene activation in many cancers.[1] Enhancers are distal regulatory elements, integrating sequence-specific transcription factor (TF) binding with recruitment of co-activators and transcriptional machinery to potentiate target gene expression.[2-5] Active enhancers are typically marked by clustered TF occupancy, high levels of H3K27ac and H3K4me1, co-ocupancy of factors such as P300/CBP, BRD4 and Mediator and bidirectional non-coding enhancer RNA (eRNA) transcription.[4,6-8] How specific TFs establish, maintain, and connect enhancers to their cognate promoters in three dimensions remains a central question in gene regulation and cancer biology.

MYB is a TF with essential roles in hematopoiesis[9-11] and multiple malignancies.[12,13] In acute leukemia, including *KMT2A*-rearranged *(KMT2A*-r) subtypes, MYB sustains oncogenic transcriptional programs, and even partial reduction leads to decreased target gene expression and loss of leukemia propagation in vivo, while sparing normal hematopoiesis.[12] This suggests a therapeutic window may exist for targeting MYB-dependent transcription in leukemia. In addition to sustaining transcriptional output, spontaneous formation of a new binding site for MYB was shown to create a novel, active enhancer that drives T-cell acute lymphoblastic leukemia (ALL),[14] at least in part by cooperating with cryptic binding sites for other TFs in the same region. MYB recruits the acetyltransferases P300/CBP to target enhancers, promoting local H3K27 acetylation and transcriptional activation. Mutations that disrupt the MYB-P300/CBP interaction impair hematopoiesis and leukemogenesis in mouse models,[15-18] and pharmacologic inhibitors of P300/CBP are advancing clinically.[19] However, whether MYB alone can initiate enhancer activity or instead functions primarily to maintain the activity of existing regulatory elements is unknown.

A key measure of enhancer function in most instances is enhancer-promoter proximity,[20-26] but it is unclear what drives these interactions. Current high-resolution 3C methods have made the striking observation that enhancer-promoter interactions are precisely localized to TF binding sites, raising the possibility that enhancer-promoter crosstalk is driven by TF interactions.[27-29] Recently, the transcription cofactor LDB1 has been shown to be essential for loop formation,[26] but it is unclear how universal this activity is among key TFs, including MYB.[30] How MYB effector function and enhancer activity are coupled, and which aspects of enhancer activity, including enhancer-promoter contact, are MYB-dependent, remain unknown. Understanding how MYB contributes to pathological enhancer function is essential for identifying both mechanistic insights and potential therapeutic vulnerabilities.

To address this knowledge gap, we investigated the function of MYB in *KMT2A*-r ALL, an aggressive malignancy with poor prognosis that remains biologically and clinically challenging despite recent therapeutic advances.[31,32] We introduced a degradation tag ($FKBP12^{F36V}$) to endogenous MYB in *KMT2A*-r ALL cells to allow rapid protein loss, resulting in significant transcriptional downregulation of known MYB target genes. Using Micro-Capture-C (MCC), we show that overall enhancer-promoter looping is maintained upon MYB degradation, but highly defined interactions at MYB-bound sites are lost, associated with decreased H3K27ac and eRNA transcription. By anchoring the Myb transactivation domain (Myb^{TA}) at a gene desert, we observed Myb^{TA}-dependent deposition of H3K27ac, increased chromatin accessibility and transcription. Remarkably, this occurred not just at the anchor site, but also at regions more than 50 kb away, likely cryptic promoters. This acetylation and transcriptional activity was abrogated or abolished by point mutations that interfere with P300/CBP binding. In addition, Myb^{TA}

induced DNA looping to facilitate 3D interactions with these transcriptionally active distal sites, as well as more long-range interactions spanning up to 400 kb. Our data argue for a role for MYB in establishing enhancers de novo, directing specific protein-protein interactions from distal regulatory elements. At a subset of MYB-bound enhancers, the continued presence of MYB is required to maintain enhancer activity and oncogene upregulation. These observations not only provide a specific model for MYB function and highlight the MYB–P300/CBP axis as a tractable therapeutic target in enhancer-driven malignancy, but also provide a paradigm for understanding enhancer function.

Materials and methods

Cell culture

Stable clones of mouse ESCs with a *TetO* array insertion (TOT2N mESC) expressing r/TetR fusion proteins were generated as described[33], and treated with 1 μg/ml doxycycline where indicated. MYB-FKBP12^{F36V} tagged SEM cells were engineered as previously described.[22] Cell lines were confirmed free from mycoplasma. See supplemental Methods for cell culture conditions and cell line generation.

Chromatin immunoprecipitation (ChIP), TOPmentation and ATAC-seq

ChIP was conducted as described previously.[34,35] ChIP-seq libraries were generated with the NEBNext Ultra II DNA library prep kit (NEB). TOPmentation was conducted as previously described.[36] ATAC-seq was conducted using Nextera Tn5 transposase (Illumina) as previously described.[37] Libraries were sequenced by 75 cycle paired-end sequencing on a NextSeq or Novaseq machine (Illumina). See supplemental Methods for protocol and data analysis details.

PolyA-minus RNA-seq and Transient Transcriptome sequencing (TT-seq)

PolyA-minus RNA was isolated using the NEBNext Poly(A) mRNA magnetic isolation module (retaining the unbound fraction). TT-seq was conducted as previously described.[35,38] Strand-specific libraries were prepared using the NEBNext Ultra II Directional RNA Library Prep Kit for Illumina (NEB) and sequenced. Data analysis details are provided in supplemental Methods.

Next Generation Capture-C and Micro-Capture-C

Capture-C ,[39,40] and Micro-Capture-C [27,41] were conducted as described previously. Capture-C analysis was performed using CapCruncher v0.2.0 and statistical analysis was performed as described.[39,40] MCC analysis was performed using the MCC pipeline.[28] See supplemental Methods for for protocol and data analysis details.[27,4127]

Results

MYB binds to active enhancers in leukemia cells

To assess the role of MYB in enhancer function, we performed genome-wide analysis in the *KMT2A*-r B-ALL cell line SEM. MYB binding was enriched at promoters and enhancers, with a pronounced preference for H3K27ac-marked active enhancers (supplemental Figure 1A),

positively correlating with enhancer-associated factors P300, BRD4 and MED1, RNAPII and H3K27ac (Figure 1A-B, supplemental Figure 1B). We Next Generation Capture-C[40] to visualize 3D interactions with the promoters of key MYB-dependent oncogenes including *BCL2*, *MYC, LMO4* and *FLT3*, identifying both intergenic and intragenic enhancers bound by MYB (Figure 1C-D, supplemental Figure 1C-D). With comparatively low levels of MYB bound at the promoters of these genes (Figure 1C-D, supplemental Figure 1C-D), this suggests an enhancer-centered role for MYB.

MYB is required for maintenance of enhancer signatures in leukemia cells

To test the requirement for MYB at enhancers, we engineered SEM cells to tag the endogenous copies of *MYB* with the $FKBP12^{F36V}$ domain (supplemental Figure 2A-C).[42] Treatment with dTAG-13 rapidly reduced MYB protein levels (Figure 2A-B, supplemental Figure 2D) and chromatin binding (Figure 2A, C, supplemental Figure 2E) at as early as 2h. Consistent with its key oncogenic role, dTAG-13 treatment dramatically decreased leukemia cell growth (supplemental Figure 2F) and colony forming potential (supplemental Figure 2G-H), although this did not appear to be driven by increased apoptosis (supplemental Figure 2I). MYB homologs A-MYB and B-MYB are only weakly expressed in SEM cells and unaffected by dTAG-13 treatment, indicating no compensatory response (supplemental Figure 2J-K).

Using TT-seq,[38] we observed widespread changes in nascent transcription after 24h MYB degradation (Figure 2D and supplemental Figure 2L), including downregulation of *BCL2*, *MYC*, *LMO4* and *CDK6* (supplemental Figure 2M). Nascent *BCL2* transcript levels decreased after as little as 2h, whereas *MYC* downregulation was more delayed (supplemental Figure 2N). We hypothesize that the much larger *MYC* enhancer (Figure 1C-D) may provide a temporal buffer for loss of MYB activity. The majority of differentially expressed genes were bound by MYB at the promoter or nearest enhancer (supplemental Figure 3A), and gene ontology analysis revealed enrichment of proliferation-related terms among downregulated genes (supplemental Figure 3B).

At MYB-bound enhancers, we saw reductions in eRNA transcription (Figure 2E, supplemental Figure 3C) and H3K27ac (Figure 2F, supplemental Figure 3D), suggesting a direct dependency on MYB for enhancer function. Decreased eRNA transcription showed a strong overlap with decreased H3K27ac and target gene downregulation, indicating functional relevance of these enhancers (Figure 2G, supplemental Figure 3E-F), exemplified by the well-characterized *BCL2* and *MYC* enhancers (Figure 2H-I).[43,44]

To determine whether the requirement for MYB is conserved beyond SEM cells, we performed siRNA-mediated *MYB* knockdown in additional leukemia models: OCI-AML3 (NPM1-mutant AML), THP-1 (*KMT2A::MLLT3* AML), and RCH-ACV (*E2A::PBX1* ALL). Efficient MYB depletion was achieved in all three cell lines (supplemental Figure 4A), with strong reductions in colony-forming potential (supplemental Figure 4B) and downregulation of key target genes (supplemental Figure 4C-E). At MYB-bound enhancers there was a clear correlation between decreases in H3K27ac and chromatin accessibility (supplemental Figure 4C–E). Together, these data demonstrate that the requirement for MYB in maintaining enhancer activity is shared across diverse leukemia contexts.

MYB is necessary for enhancer-promoter interactions at endogenous loci

Given the loss of enhancer activity associated with MYB degradation, we used the high-resolution 3C technique MCC[27] to determine if MYB contributes to spatial co-localisation of enhancers and promoters. This revealed sharp, high frequency enhancer-promoter interaction peaks (MCC peaks), not visible using the lower-resolution Capture-C (Figure 3A-D, supplemental Figure 5A-B). We have previously shown that the oncogene *FLT3* is regulated by a broad KMT2A-AFF1-dependent enhancer within the neighbouring *PAN3*.[36] In addition to the broad interaction profile seen with Capture-C, we observed two prominent MCC peaks adjacent to this enhancer, one closely overlapping with MYB binding (Figure 3C-D). Similar MYB-bound promoter-interacting peaks were present at the enhancers of *BCL2* and *MYC* (Figure 3A-B, supplemental Figure 5A-B). While not all promoter-interacting sites were bound by MYB, MYB binding within enhancers often co-localized with MCC peaks. Across a panel of 43 genes, including known MYB-target oncogenes and transcriptional regulators that are recurrently implicated in KMT2A-driven leukemogenesis (supplemental Table 1), we found overlap between MYB and MCC peaks at most loci (supplemental Figure 5C).

MYB degradation had little or no effect on the frequency of enhancer-promoter interaction for the majority of MCC peaks (supplemental Figure 5D). However, at MYB-bound peaks, we observed a strong bias towards decreased interaction frequency (Figure 3E), with statistically significant peaks exclusively losing interactions (Figure 3F). Decreased interaction sites were bound by much higher levels of MYB (Figure 3G) and enriched for key enhancer proteins P300, BRD4 and MED1 (supplemental Figure 5E). Importantly, decreased interaction frequency following MYB degradation correlated with loss of H3K27ac and chromatin accessibility (Figure 3H, supplemental Figure 5G-H). Finally, the majority of genes that lost promoter interactions with MYB-bound MCC peaks were downregulated (Figure 3I). Together, these results reveal a role for MYB in gene activation via maintenance of enhancer activity and promoter interactions.

These features are clearly demonstrated at *BCL2*, with major decreases in enhancer-promoter contact at MYB-bound loci (Figure 3A-B, see MCC differential track), which also show reduced H3K27ac, chromatin accessibility and eRNA transcription (Figure 2H, 3B). Thus, the presence of MYB is required for localized contact with the *BCL2* promoter, along with enhancer activity and gene expression. Similar effects were observed at the *FLT3* and *MYC* enhancers (Figure 3C-D, 2I, supplemental Figure 5A-B).

For a subset of MYB-dependent MCC interactions, e.g. at the *MYC* enhancer (supplemental Figure 5A-B), we observed co-occupancy of the architectural proteins CTCF and/or RAD21. However, this association was not replicated globally or in a systematic analysis of MYB-bound MCC interaction sites, with ~85% of MYB peaks not bound by CTCF or RAD21 (supplemental Figure 6A-B). Furthermore, CTCF and RAD21 chromatin binding were not affected by MYB degradation (supplemental Figure 6C-D). Together, thise supports a model in which MYB regulates enhancer–promoter communication largely independently of CTCF/RAD21.

To understand the dynamics of MYB enhancer regulation, we repeated our chromatin analyses at a 2h timepoint, to look at the acute consequences of MYB loss, and following a subsequent 24h washout of dTAG-13, to study the effects of MYB recovery (supplemental Figure 7A-C). After 2h, H3K27ac levels at MYB-bound enhancers were already reduced, although the decrease was not as great as at 24h (supplemental Figure 7D), and levels mostly recovered after washout. We saw a comparable effect on MYB-dependent transcription, where gene expression changes at 24h correlated with a more muted effect at 2h, but were restored after washout (supplemental Figure

7E). Similarly, reductions in enhancer-promoter interactions were overall more subtle at 2h (supplemental Figure 7F), although H3K27ac losses at these sites were already pronounced (supplemental Figure 7G). While many MCC interactions had not yet decreased at 2h, we found clear losses at key sensitive genes. The *BCL2* and *CXCR4* enhancers showed obvious reductions in H3K27ac, chromatin accessibility and promoter interactions after 2h dTAG-13 treatment, consistent with the early transcriptional downregulation of *BCL2* (supplemental Figure 2J). Following dTAG washout and restoration of MYB binding at the enhancers, these features recovered (supplemental Figure 7H-I). This argues that, at these loci, MYB is required for maintenance of, and capable of establishing, enhancer activity.

Finally, to validate our findings in another leukemia model, we conducted MCC in OCI-AML3 cells after *MYB* knockdown, observing a loss of promoter interactions at a subset of MYB-bound loci (Figure 4A). As in SEM cells, reduction in interaction frequency closely correlated with reduced H3K27ac and chromatin accessibility (Figure 4B-C). For example, at *BCL2* and *MYC* (Figure 4D-E), MYB-bound enhancer loci showed decreases in H3K27ac, chromatin accessibility and promoter interaction frequency following *MYB* knockdown, associated with decreased expression (supplementary Figure 4C). Overall, these results demonstrate that MYB is required for key enhancer activities, including H3K27ac, eRNA transcription and physical proximity with the target gene promoter. Loss of these features results in transcriptional downregulation of target genes. We therefore sought to determine if binding of MYB alone is sufficient to generate an enhancer.

Myb^{TA} is sufficient to initiate de novo enhancer activity

Most attempts to explore TF function have focussed on endogenous enhancers, with additional TF binding sites present, or used exogenous constructs lacking a chromatin environment. We wanted to determine if binding of MYB alone could generate enhancers de novo in a chromatin context. We used a well-characterized chromatin anchoring system, based on an array of *Tet operator* (*TetO*) sequences flanked by inert human chromatin (*TetO* BAC) inserted into mESCs.[33,35,36] By fusing Myb to the Tet repressor (TetR) DNA binding domain (Figure 5A), we tethered the TF to the *TetO* locus (Figure 5B). Since the activity of MYB may be attenuated through intramolecular interactions between its N- and C-termini, we isolated the transactivation (TA) domain of mouse Myb (Myb^{TA}), which is sufficient for activity.[45-47]

Binding of both TetR-Myb^{TA} and the control TetR-only was restricted to the *TetO* locus (Figure 5C-D). TetR-Myb^{TA} recruited its co-activator p300 (Figure 5C), resulting in H3K27ac enrichment, in a region previously devoid of this modification (Figure 5E, supplemental Figure 8A). Additionally, we found a higher ratio of H3K4me1 to H3K4me3, a hallmark of enhancers[6,48] (supplemental Figure 8A), and localisation of Brd4 and Mediator (Figure 5C, supplemental Figure 8B). We also saw TetR-Myb^{TA}-dependent binding of Tbp and RNAPII, suggesting the potential for transcription initiation (Figure 5C, supplemental Figure 8B). Together, this indicates that TetR-Myb^{TA} binding at the *TetO* locus generated an enhancer-like element.

We performed RNA-seq of polyA-depleted transcripts to look for nascent transcription (Figure 5F). Remarkably, in cells expressing TetR-Myb^{TA}, we detected transcription on both strands throughout the ~150 kb region centered on *TetO*, which was previously transcriptionally silent. While some may have initiated at *TetO* itself, much appeared to originate at sites up to 50 kb away from the TetR-Myb^{TA} binding site.

We next used ATAC-seq to identify accessible regions that could be sites of transcription initiation. While some ATAC-seq peaks were visible in cells expressing no TetR protein or TetR alone (*L1*, *L3* and *L4*), accessibility increased upon expression of TetR-Myb^{TA}, along with the appearance of a novel ATAC-seq peak (*L2*) (Figure 5G). Strikingly, unique to TetR-Myb^{TA} expressing cells, we observed H3K27ac enrichment at all four loci, suggesting distal activation by TetR-Myb^{TA} binding at *TetO* (Figure 5E, H, supplemental Figure 8C). Motif analysis indicated *L1-L4* contain putative TF binding sites, but with no common factors (supplemental Figure 8D). *L1* and *L3* appeared to be origins of bidirectional transcription, consistent with enhancer-like activity, while transcription from *L2* and *L4* was directionally biased, reminiscent of promoters (Figure 5F, supplemental Figure 8C). Consistent with this, *L1* and *L3* were enriched for the enhancer mark H3K4me1, whereas *L2* and *L4* were associated with the promoter modification H3K4me3 (Figure 5H). This was specifically induced in TetR-Myb^{TA} expressing cells. Taken together, these data strongly argue that binding of TetR-Myb^{TA} in isolation establishes an enhancer-like element capable of activating distant cryptic promoters and enhancers.

Myb^{TA} binding induces – and is necessary for – chromatin looping

Given the effect of MYB loss on enhancer-promoter interactions in SEM and OCI-AML3 cells, we hypothesized that Myb binding may induce contact between *TetO* and distal loci to activate them. We exploited the properties of the Tet-On/Tet-Off systems;[49] on addition of doxycycline, binding of TetR-Myb^{TA} to *TetO* is disrupted, whereas rTetR-Myb^{TA} only binds in the presence of doxycycline. We performed Capture-C in rTetR-Myb^{TA} cells, using a *TetO* specific capture probe to measure interactions with the enhancer-like element (Figure 6A). In the absence of rTetR-Myb^{TA} binding (no Dox) we observed a normal decay in interaction frequency on either side of *TetO* (Figure 6A), indicating random chromatin interactions. However, within 30 min of doxycycline-induced binding of rTetR-Myb^{TA}, chromatin interactions appeared between *TetO* and *L1, L3* and *L4* (supplemental Figure 9A-B). *L2* is only 14.5 kb from *TetO*, so this interaction may be obscured by proximity to the capture locus. We also detected interactions up to 400 kb away from *TetO* (highlighted in gray, Figure 6A). Confirming our endogenous MYB degradation experiments, many of these interactions were lost following TetR-Myb^{TA} displacement upon doxycycline treatment, arguing that Myb is responsible for establishing, and required to maintain, chromatin interactions (Figure 6A, supplemental Figure 9A). This is particularly striking at *L3* (supplemental Figure 9A), which is marked with high levels of TetR-Myb^{TA}-dependent H3K27ac and H3K4me1 (Figure 5E, H). Together, our data argue that MYB is capable of remodelling large chromatin domains, driving productive interactions to induce transcription at distal loci, likely through cooperation with other factors at distal sites.

We performed ChIP-seq for Ctcf and the cohesin subunit Rad21 to ask whether the long-range interactions were driven by architectural proteins. Within the *TetO* BAC, Ctcf binding was detected in both TetR-only and TetR-Myb^{TA} cells in a doxycycline-sensitive manner, implying recruitment driven by increased accessibility at the *TetO*, independent of Myb^{TA} (supplemental Figure 9B-C). In contrast, Rad21 binding was maintained in the presence of doxycycline, despite the loss of looping (supplemental Figure 9A, D). Similar behavior was seen across a ~1.8 Mb window flanking the *TetO* insertion, with TetR-induced, doxycycline-insensitive binding of Ctcf/Rad21 (supplemental Figure 10A-B). From this, we conclude that Ctcf and/or cohesin alone are insufficient for the looping observed, although we cannot exclude a role in facilitating TetR-Myb^{TA}-dependent interactions at these loci.

Enhancer activity is dependent on continued presence of Myb^{TA} and p300/Cbp

To understand the kinetics of Myb^{TA}-dependent enhancer activation, we used acute doxycycline treatment of rTetR-Myb^{TA}-expressing mESCs, observing rapid induction of transcription from *TetO* as well as *L1-4* within 30 min, with further increases at 24h (Figure 6B). Of interest, the early onset of transcription appeared to precede H3K27ac deposition (Figure 6B, supplemental Figure 11A), suggesting that appreciable H3K27ac levels may be unnecessary for transcription initiation.

We used doxycycline treatment in TetR-Myb^{TA} cells to test the requirement for TetR-Myb^{TA} in enhancer maintenance. A 1h treatment with doxycycline, which abrogated TetR-Myb^{TA} binding, resulted in a dramatic loss of transcription and H3K27ac from *TetO* and the distal loci (Figure 6C, supplemental Figure 11B). Thus, consistent with our MYB degradation experiments, local and distal enhancer activity are absolutely dependent on continued presence of TetR-Myb^{TA} at *TetO*.

Finally, we probed the role of p300/Cbp at this locus using Myb^{TA} mutants that partially (M303V) or fully (L302A) disrupt binding to p300/Cbp.[15,50,51] TetR-Myb^{TA}L302A localized to *TetO*, but did not result recruit p300 and was unable to induce detectable H3K27ac or transcription at *TetO* or *L1-4* (Figure 6D, supplemental Figure 6D). In contrast, M303V partially reduced, but did not eliminate, p300 binding and H3K27ac deposition (Figure 6D, supplemental Figure 11C). Strikingly, transcription was dramatically reduced with both mutations, to ~1% of TetR-Myb^{TA} levels (Figure 6D). Thus, stable p300/Cbp recruitment via Myb^{TA} is required for robust transcriptional output at this enhancer-like element.

Discussion

We show that MYB binding sustains transcription by maintaining precise enhancer-promoter interactions and enhancer activity at key leukemia-associated genes. To determine if MYB is sufficient to establish de novo enhancer-like regions, we anchored Myb^{TA} in a gene desert. Myb^{TA} alone recruited co-activators, induced long-range interactions, activating cryptic promoters, and was required to maintain these interactions, suggesting that mediating long-range gene activation is an intrinsic property of MYB. How it selects sites for activation is unclear. It is likely context dependent, as regulatory elements can retain function when removed from their endogenous context, but remain responsive to the overall cell environment.[52] Indeed, we observed low-level chromatin accessibility in the absence of TetR-Myb^{TA}, indicating the potential for these sites to be bound by other TFs, poised for activation upon interaction with Myb, although motif analysis did not identify an obvious candidate. These findings suggest that MYB can drive activation of minimally active cryptic elements to create functional regulatory domains.

While LDB1 is essential for loop formation,[26] recent high-resolution 3C-based observations have suggested that many TF binding sites could be nucleation points for enhancer-promoter interactions.[27-29] Our data extend these findings by showing that MYB degradation disrupts many interactions precisely localized at MYB-bound loci, suggesting that MYB itself (or the co-activators it recruits) drives enhancer-promoter contact in these regions. These effects are not uniform across all MYB binding sites; at many MYB-bound enhancers, MYB degradation had little or no effect on promoter interaction. This argues that an essential requirement for MYB is

context specific, perhaps reflecting the absence of alternative, redundant factors. We cannot exclude a role for MYB homologs A/B-MYB, although they are lowly expressed in SEM cells. Futhermore, where MYB degradation reduced the punctate interaction at the MYB peak, the broader interaction profile of the enhancer remained intact, and overall promoter-enhancer interactions continued in the absence of MYB. Thus at most enhancers, no single TF drives the interaction profile, but instead interactions combine across multiple protein complexes. Future work will determine if this is the function of a handful of key factors such as MYB and LDB1, or if all TFs contribute to enhancer-promoter crosstalk.

While we cannot exclude a role for Ctcf and/or cohesin in the Myb^{TA}-driven interactions we observe, the limited overlap between CTCF/RAD21 and MYB in SEM cells argues against this as the primary mechanism driving MYB-dependent looping. Instead, we suggest that MYB-dependent enhancer-promoter interactions are likely driven by co-activator recruitment, possibly in concert with other TFs, and subsequent RNAPII complex stabilisation. MYB is known to function via P300/CBP,[15-17] which may provide a mechanism for enhancer-promoter interactions. Upon MYB degradation, H3K27ac and interaction frequency reductions correlated at MYB-bound enhancers, although acetylation loss appeared to precede structural changes. It is unclear whether this reflects independent or interdependent MYB activities. Using mutations that disrupt Myb-p300/Cbp interactions,[15,50,51] we observed reduced H3K27ac at *TetO* and distal transcription. Strikingly, the transcriptional decrease was much more dramatic, indicating acetyltransferase-independent p300/Cbp functions, or additional Myb^{TA}-interacting cofactors contributing to activation of distal loci. There is no intrinsic requirement for enhancer-promoter contact and promoter driven transcription to be controlled by the same process; we previously found that degradation of BRD4 disrupts transcription without affecting enhancer-promoter interactions.[44] In our system, MYB appears sufficient for both. Further work is required to explore how this is mediated.

In the context of leukemia, our results provide a mechanistic rationale for the oncogenic function of MYB. Previous studies have implicated MYB in transcriptional activation and enhancer occupancy, but here we reveal that enhancer activity, chromatin looping, and transcriptional output are acutely dependent on continued MYB presence. This dual capacity – maintaining and establishing enhancers – may explain its involvement in enhancer hijacking and necessity to sustain the leukemia phenotype.

Our work underscores the therapeutic vulnerability of MYB-driven enhancer programs and suggests that targeting MYB or its co-activator interactions (e.g., via P300/CBP inhibitors[53]) could disrupt layers of leukemic transcriptional regulation. Mutational analysis of the MYB-P300 interface revealed that transcriptional activation is more sensitive to disruption than histone acetylation, indicating additional layers of enhancer activation that may involve non-enzymatic co-factors or scaffolding roles. This positions MYB as a master regulator of leukemia-specific enhancer function, with implications for basic enhancer biology and therapeutic targeting of MYB-dependent malignancies.

Acknowledgments

TAM, NEJ and ALS were supported by the Medical Research Council (MRC, UK) (Molecular Haematology Unit grant MC_UU_00016/6 and MC_UU_00029/6). GB, VS and CC were supported by Wellcome Trust studentships. I-JL was funded with an MRC Clinical Research Training Fellowship (MR/M003221/1) and Anya Sturdy Charitable Trust for Medical Research Fellowship (A130320/129280). NTC was supported by a Kay Kendall Leukemia Fund Intermediate Fellowship (KKL1443). ND was funded by Cancer Research UK (SEBCATP-2022/100011). JOJD and HL were funded by the Lister Institute, MRC (Molecular Haematology Unit grant MC_UU_00029/04), Wellcome Trust (225220/Z/22/Z), Oxford National Institute of Health Research Biomedical Research Centre (NIHR203311). PV was supported by the MRC (Molecular Haematology Unit grant MC_UU_00029/8) and Blood Cancer UK Programme Continuity Grant (13008). JRH was supported by Medical Research Council (MRC) MHU grants MC_UU_00016/14 and MC_UU_00029/3.

Author Contributions

Conceptualization: I-JL, NTC and TAM. Methodology: I-JL, NTC and TAM. Investigation: I-JL, GB, VS, ND, HL, NEJ and NTC. Formal analysis: I-JL, ALS, JRHarman, CC, JCH and NTC. Funding acquisition: TAM. Supervision: PV, JOJD, JRHughes and TAM. Writing – Original Draft: I-JL, NTC and TAM Writing – Review & Editing: all authors.

Conflict of Interest Disclosures

TAM is a paid consultant for and shareholder in Dark Blue Therapeutics Ltd. JOJD and JRHughes are founders of and paid consultants for Nucleome Therapeutics. JRHughes holds patents for Capture-C (WO2017068379A1, EP3365464B1, US10934578B2). The remaining authors declare no competing interests.

References

1. Loven J, Hoke HA, Lin CY, et al. Selective inhibition of tumor oncogenes by disruption of super-enhancers. *Cell*. 2013;153(2):320-334.
2. Long Hannah K, Prescott Sara L, Wysocka J. Ever-Changing Landscapes: Transcriptional Enhancers in Development and Evolution. *Cell*. 2016;167(5):1170--1187.
3. Kassouf M, Ford S, Blayney J, Higgs D. Understanding fundamental principles of enhancer biology at a model locus: Analysing the structure and function of an enhancer cluster at the alpha-globin locus. *Bioessays*. 2023;45(10):e2300047.
4. Yang JH, Hansen AS. Enhancer selectivity in space and time: from enhancer-promoter interactions to promoter activation. *Nat Rev Mol Cell Biol*. 2024.
5. Whyte Warren A, Orlando David A, Hnisz D, et al. Master Transcription Factors and Mediator Establish Super-Enhancers at Key Cell Identity Genes. *Cell*. 2013;153(2):307--319.
6. Heintzman ND, Stuart RK, Hon G, et al. Distinct and predictive chromatin signatures of transcriptional promoters and enhancers in the human genome. *Nat Genet*. 2007;39(3):311-318.
7. Zhang T, Zhang Z, Dong Q, Xiong J, Zhu B. Histone H3K27 acetylation is dispensable for enhancer activity in mouse embryonic stem cells. *Genome Biol*. 2020;21(1):45.
8. Creyghton MP, Cheng AW, Welstead GG, et al. Histone H3K27ac separates active from poised enhancers and predicts developmental state. *Proc Natl Acad Sci U S A*. 2010;107(50):21931-21936.
9. Mucenski ML, McLain K, Kier AB, et al. A functional c-myb gene is required for normal murine fetal hepatic hematopoiesis. *Cell*. 1991;65(4):677--689.
10. Sumner R, Crawford A, Mucenski M, Frampton J. Initiation of adult myelopoiesis can occur in the absence of c-Myb whereas subsequent development is strictly dependent on the transcription factor. *Oncogene*. 2000;19(30):3335--3342.
11. Sakamoto H, Dai G, Tsujino K, et al. Proper levels of c-Myb are discretely defined at distinct steps of hematopoietic cell development. *Blood*. 2006;108(3):896--903.
12. Zuber J, Rappaport AR, Luo W, et al. An integrated approach to dissecting oncogene addiction implicates a Myb-coordinated self-renewal program as essential for leukemia maintenance. *Genes \& Development*. 2011;25(15):1628--1640.
13. Biersack B, Höpfner M. Emerging role of MYB transcription factors in cancer drug resistance. *Cancer Drug Resist*. 2024;7:15.
14. Mansour MR, Abraham BJ, Anders L, et al. An oncogenic super-enhancer formed through somatic mutation of a noncoding intergenic element. *Science*. 2014;346(6215):1373--1377.
15. Sandberg ML, Sutton SE, Pletcher MT, et al. c-Myb and p300 Regulate Hematopoietic Stem Cell Proliferation and Differentiation. *Developmental Cell*. 2005;8(2):153--166.
16. Dai P, Akimaru H, Tanaka Y, et al. CBP as a transcriptional coactivator of c-Myb. *Genes & Development*. 1996;10(5):528--540.
17. Pattabiraman DR, Sun J, Dowhan DH, Ishii S, Gonda TJ. Mutations in Multiple Domains of c-Myb Disrupt Interaction with CBP/p300 and Abrogate Myeloid Transforming Ability. *Molecular Cancer Research*. 2009;7(9):1477--1486.
18. Papathanasiou P, Tunningley R, Pattabiraman DR, et al. A recessive screen for genes regulating hematopoietic stem cells. *Blood*. 2010;116(26):5849--5858.

19. Wu X, Zhang X, Tang S, Wang Y. The important role of the histone acetyltransferases p300/CBP in cancer and the promising anticancer effects of p300/CBP inhibitors. *Cell Biol Toxicol*. 2025;41(1):32.
20. Sanyal A, Lajoie BR, Jain G, Dekker J. The long-range interaction landscape of gene promoters. *Nature*. 2012;489(7414):109-113.
21. Furlong EEM, Levine M. Developmental enhancers and chromosome topology. *Science*. 2018;361(6409):1341--1345.
22. Hyle J, Zhang Y, Wright S, et al. Acute depletion of CTCF directly affects MYC regulation through loss of enhancer-promoter looping. *Nucleic Acids Res*. 2019;47(13):6699-6713.
23. Chen LF, Lee J, Boettiger A. Recent progress and challenges in single-cell imaging of enhancer-promoter interaction. *Curr Opin Genet Dev*. 2023;79:102023.
24. Chen Z, Snetkova V, Bower G, et al. Increased enhancer-promoter interactions during developmental enhancer activation in mammals. *Nat Genet*. 2024;56(4):675-685.
25. Pollex T, Marco-Ferreres R, Ciglar L, et al. Chromatin gene-gene loops support the cross-regulation of genes with related function. *Mol Cell*. 2024;84(5):822-838.e828.
26. Aboreden NG, Lam JC, Goel VY, et al. LDB1 establishes multi-enhancer networks to regulate gene expression. *Mol Cell*. 2025;85(2):376-393 e379.
27. Hua P, Badat M, Hanssen LLP, et al. Defining genome architecture at base-pair resolution. *Nature*. 2021;595(7865):125--129.
28. Maresca M, Brand T, Li H, Teunissen H, Davies J, Wit E. Pioneer activity distinguishes activating from non-activating SOX2 binding sites. *The EMBO Journal*. 2023:e113150.
29. Goel VY, Huseyin MK, Hansen AS. Region Capture Micro-C reveals coalescence of enhancers and promoters into nested microcompartments. *Nat Genet*. 2023;55(6):1048-1056.
30. Agarwal A, Korsak S, Choudhury A, Plewczynski D. The dynamic role of cohesin in maintaining human genome architecture. *Bioessays*. 2023;45(10):e2200240.
31. Rice S, Roy A. MLL-rearranged infant leukaemia: A 'thorn in the side' of a remarkable success story. *Biochim Biophys Acta Gene Regul Mech*. 2020;1863(8):194564.
32. Nguyen K, Devidas M, Cheng SC, et al. Factors influencing survival after relapse from acute lymphoblastic leukemia: a Children's Oncology Group study. *Leukemia*. 2008;22(12):2142-2150.
33. Blackledge NP, Farcas AM, Kondo T, et al. Variant PRC1 complex-dependent H2A ubiquitylation drives PRC2 recruitment and polycomb domain formation. *Cell*. 2014;157(6):1445-1459.
34. Godfrey L, Crump NT, Thorne R, et al. DOT1L inhibition reveals a distinct subset of enhancers dependent on H3K79 methylation. *Nature Communications*. 2019;10(1):2803.
35. Kerry J, Godfrey L, Repapi E, et al. MLL-AF4 Spreading Identifies Binding Sites that Are Distinct from Super-Enhancers and that Govern Sensitivity to DOT1L Inhibition in Leukemia. *Cell Reports*. 2017;18(2):482--495.
36. Crump NT, Smith AL, Godfrey L, et al. MLL-AF4 cooperates with PAF1 and FACT to drive high-density enhancer interactions in leukemia. *Nat Commun*. 2023;14(1):5208.
37. Buenrostro JD, Giresi PG, Zaba LC, Chang HY, Greenleaf WJ. Transposition of native chromatin for fast and sensitive epigenomic profiling of open chromatin, DNA-binding proteins and nucleosome position. *Nature Methods*. 2013;10(12):1213--1218.
38. Schwalb B, Michel M, Zacher B, et al. TT-seq maps the human transient transcriptome. *Science*. 2016;352(6290):1225--1228.

39. Downes DJ, Smith AL, Karpinska MA, et al. Capture-C: a modular and flexible approach for high-resolution chromosome conformation capture. *Nat Protoc*. 2022;17(2):445-475.
40. Davies JOJ, Telenius JM, McGowan SJ, et al. Multiplexed analysis of chromosome conformation at vastly improved sensitivity. *Nature Methods*. 2016;13(1):74--80.
41. Hamley JC, Li H, Denny N, Downes D, Davies JOJ. Determining chromatin architecture with Micro Capture-C. *Nat Protoc*. 2023;18(6):1687-1711.
42. Nabet B, Roberts JM, Buckley DL, et al. The dTAG system for immediate and target-specific protein degradation. *Nat Chem Biol*. 2018;14(5):431-441.
43. Benito JM, Godfrey L, Kojima K, et al. MLL-Rearranged Acute Lymphoblastic Leukemias Activate BCL-2 through H3K79 Methylation and Are Sensitive to the BCL-2-Specific Antagonist ABT-199. *Cell Rep*. 2015;13(12):2715-2727.
44. Crump NT, Ballabio E, Godfrey L, et al. BET inhibition disrupts transcription but retains enhancer-promoter contact. *Nature Communications*. 2021;12(1):223.
45. Sakura H, Kanei-Ishii C, Nagase T, Nakagoshi H, Gonda TJ, Ishii S. Delineation of three functional domains of the transcriptional activator encoded by the c-myb protooncogene. *Proceedings of the National Academy of Sciences*. 1989;86(15):5758--5762.
46. Weston K, Bishop JM. Transcriptional activation by the v-myb oncogene and its cellular progenitor, c-myb. *Cell*. 1989;58(1):85--93.
47. Kalkbrenner F, Guehmann S, Moelling K. Transcriptional activation by human c-myb and v-myb genes. *Oncogene*. 1990;5(5):657-661.
48. Ernst J, Kheradpour P, Mikkelsen TS, et al. Mapping and analysis of chromatin state dynamics in nine human cell types. *Nature*. 2011;473(7345):43-49.
49. Gossen M, Freundlieb S, Bender G, Müller G, Hillen W, Bujard H. Transcriptional Activation by Tetracyclines in Mammalian Cells. *Science*. 1995;268(5218):1766--1769.
50. Parker D, Rivera M, Zor T, et al. Role of Secondary Structure in Discrimination between Constitutive and Inducible Activators. *Molecular and Cellular Biology*. 1999;19(8):5601--5607.
51. Zor T, Guzman RND, Dyson HJ, Wright PE. Solution Structure of the KIX Domain of CBP Bound to the Transactivation Domain of c-Myb. *Journal of Molecular Biology*. 2004;337(3):521--534.
52. Georgiades E, Harrold CL, Roberts N, et al. Active regulatory elements recruit cohesin to establish cell-specific chromatin domains. *bioRxiv*. 2023:2023.2010.2013.562171.
53. Nicosia L, Spencer GJ, Brooks N, et al. Therapeutic targeting of EP300/CBP by bromodomain inhibition in hematologic malignancies. *Cancer Cell*. 2023;41(12):2136-2153.e2113.

Figure Legends

Figure 1. MYB binds to active enhancers in leukemia cells. (**A**) Spearman correlation coefficients for ChIP-seq data at enhancer ATAC-seq peaks in SEM cells. (**B**) Heatmap comparing levels of histone modifications and chromatin binding of MYB and co-activator proteins at enhancer ATAC-seq peaks in SEM cells. Peaks are ranked based on accessibility. (**C**) Capture-C, ChIP-seq and ATAC-seq at the *BCL2* gene and enhancer region (labelled E) in SEM cells. Capture-C shows the frequency of interactions with the *BCL2* promoter (labelled P), indicated by the vertical gray bar, and is displayed as the mean of three biological replicates. Upper track shows Capture-C for the broad locus, with an expanded view below. (**D**) Capture-C, ChIP-seq, and ATAC-seq data at *MYC* as in (C).

Figure 2. MYB is required for maintenance of enhancer signatures in leukemia cells. (**A**) Western blot for MYB in MYB-FKBP12^{F36V} tagged SEM cells following addition of 0.5 μM dTAG-13. Cells were fractionated, with GAPDH and MENIN used as loading controls for the whole cell and chromatin-bound fractions. Representative of three biological replicates. (**B**) Quantification of whole cell protein western blot following dTAG-13 treatment. Error bars represent the standard deviation from four biological replicates, **p<0.01; ****p<0.0001. (**C**) Mean MYB CUT&Tag signal at MYB-bound enhancers in control (untreated) and 24h dTAG-13-treated MYB-FKBP12^{F36V} tagged SEM cells. (**D**) Changes in TT-seq RNA levels following 24h treatment with dTAG-13 in MYB-FKBP12^{F36V} tagged SEM cells. Statistically significant differences from three biological replicates, FDR < 0.05. (**E**) Strand-specific TT-seq levels at intergenic MYB-bound and non-MYB-bound enhancers and all intergenic enhancer ATAC-seq peaks, in control (untreated) and 24h dTAG-13-treated MYB-FKBP12^{F36V} tagged SEM cells. Lines represent mean, shading represents ± SEM, n = 3 independent experiments. (**F**) Mean distribution of H3K27ac at MYB-bound and all enhancer ATAC peaks in control (untreated) and 24h dTAG-13-treated MYB-FKBP12^{F36V} tagged SEM cells. (**G**) Proportion of intergenic enhancers with differential eRNA expression following dTAG-13 treatment that are associated with differentially expressed target genes. MYB and H3K27ac ChIP-seq, TT-seq and ATAC-seq at MYB-bound enhancers for (**H**) *BCL2* and (**I**) *MYC* in MYB-FKBP12^{F36V} tagged SEM cells, with or without the addition of dTAG-13 for 24h. Differential tracks show the difference in interaction frequency between DMSO and dTAG-13 conditions (dTAG-13 minus DMSO). MYB peaks are annotated in red.

Figure 3. MYB is necessary for maintenance of enhancer-promoter interactions at endogenous loci. Capture-C and ChIP-seq in SEM cells, and Micro-Capture-C (MCC), CUT&Tag, ATAC-seq and TT-seq in MYB-FKBP12^{F36V} tagged SEM cells, with or without the addition of dTAG-13 for 24h at the (**A**) *BCL2* and (**C**) *FLT3* loci. Enhancer regions are highlighted by the green line labelled E. Enlarged views of regions within the *BCL2* (**B**) and *FLT3* (**D**) enhancers are highlighted by gray gradient boxes and their relative positions within the enhancers annotated by gray horizontal lines. Capture-C and MCC traces are scaled to emphasize distal interactions. Differential tracks show the difference between DMSO and dTAG-13 conditions (dTAG-13 minus DMSO). (**E**) Change in MCC interaction frequency (mean logFC of three replicates) between promoters and ATAC, MYB, CTCF, RAD21 and P300 peaks within approx. 500 kb of the capture point following the addition of dTAG-13 for 24h. Violin plot

shows frequency distribution. (**F**) Changes in MCC interaction frequency at MYB peaks following 24h treatment with dTAG-13 in MYB-FKBP12^{F36V} tagged SEM cells. Statistically significant differences from three biological replicates, FDR < 0.05. (**G**) Mean MYB CUT&Tag signal at MYB-bound decreased or unchanged MCC interaction sites in control (untreated) and 24h dTAG-13-treated MYB-FKBP12^{F36V} tagged SEM cells. (**H**) Change in MCC interaction frequency, ATAC-seq and H3K27ac levels at MYB peaks associated with decreased or unchanged MCC interactions. (**I**) Correlation of loss of MCC interaction at MYB peak with changes in gene expression.

Figure 4. MYB is required for enhancer activity in OCI-AML3 cells. (**A**) Changes in MCC interaction frequency following 24h MYB knockdown in OCI-AML3 cells. Statistically significant differences from three biological replicates, FDR < 0.05. (**B**) Change in MCC interaction frequency at ATAC-seq peaks associated with differential accessibility following 24h MYB knockdown in OCI-AML3 cells. (**C**) Change in MCC interaction frequency, ATAC-seq and H3K27ac levels at MYB peaks associated with decreased or unchanged MCC interactions. MCC, MYB and H3K27ac CUT&Tag and ATAC-seq in OCI-AML3 cells under control (non-targeting) or 24h MYB knockdown (KD) conditions at BCL2 (**D**) and MYC (**E**). Differential tracks show the difference between control and KD conditions (KD minus control).

Figure 5. TetR-MYB^{TA} is sufficient to initiate de novo enhancer activity. (**A**) MYB schematic, with tandem repeats R1-3 of the DNA binding (DB) domain, the transactivation (TA) domain and the negative regulatory (NR) domain, as well as r/TetR-Myb^{TA} and control (r/TetR only) proteins. (**B**) Targeting of factors to *TetO* via the r/TetR DNA-binding domain. Doxycycline disrupts DNA binding of TetR but induces binding of rTetR. (**C**) ChIP-qPCR analysis across the *TetO*-containing locus in cell lines stably expressing either TetR or TetR-Myb^{TA}, using antibodies against the indicated proteins. Error bars represent the standard deviation from three biological replicates. (**D**) TetR ChIP-seq, (**E**) H3K27ac ChIP-seq, (**F**) Poly-A minus RNA-seq and (**G**) ATAC-seq at the integrated *TetO* array. *L1-4* are highlighted in gray. (**H**) ChIP-qPCR for H3K27ac (left), H3K4me1 (middle) and H3K4me3 (right) at *L1-4* in cells expressing TetR (black bars) or TetR-Myb^{TA} (colored bars). Error bars represent the standard deviation from three biological replicates.

Figure 6. MYB^{TA} binding induces – and is necessary for – chromatin looping. (**A**) Capture-C and H3K27ac ChIP-seq in untreated and doxycycline-treated rTetR-Myb^{TA} and TetR-Myb^{TA} expressing cells across the *TetO* locus. Differential tracks show the difference in interaction frequency between untreated and doxycycline conditions. (**B**) ChIP-qPCR analysis in rTetR-Myb^{TA} expressing cells for rTetR (1st panel) and H3K27ac (2nd panel) and qRT-PCR analysis of cDNA generated from total RNA (3rd panel) across the TetO-containing locus (±0.5 kb, ±1 kb, and ±5 kb from the *TetO* locus) (3rd panel) and at *L1-4* (4th panel) following doxycycline treatment for 0.5 and 24h. qRT-PCR data were normalized to *Gapdh* expression. Error bars represent the standard deviation from three biological replicates. (**C**) As in (B), ChIP-qPCR and qRT-PCR in TetR-Myb^{TA} expressing cells following doxycycline treatment for 1h. (**D**) ChIP-qPCR analysis for H3K27ac across the *TetO* containing locus in cell lines stably expressing either TetR-Myb^{TA} (gray), TetR-Myb^{TA}M303V (pink), or TetR-Myb^{TA}L302A (blue) (1st panel), qRT-PCR analysis of cDNA generated from total RNA across the *TetO* containing locus (2nd and

3rd panel) and at *L1-4* (4th panel), normalized to *Rn18s*. Representative of three biological replicates.

5

Figure 1

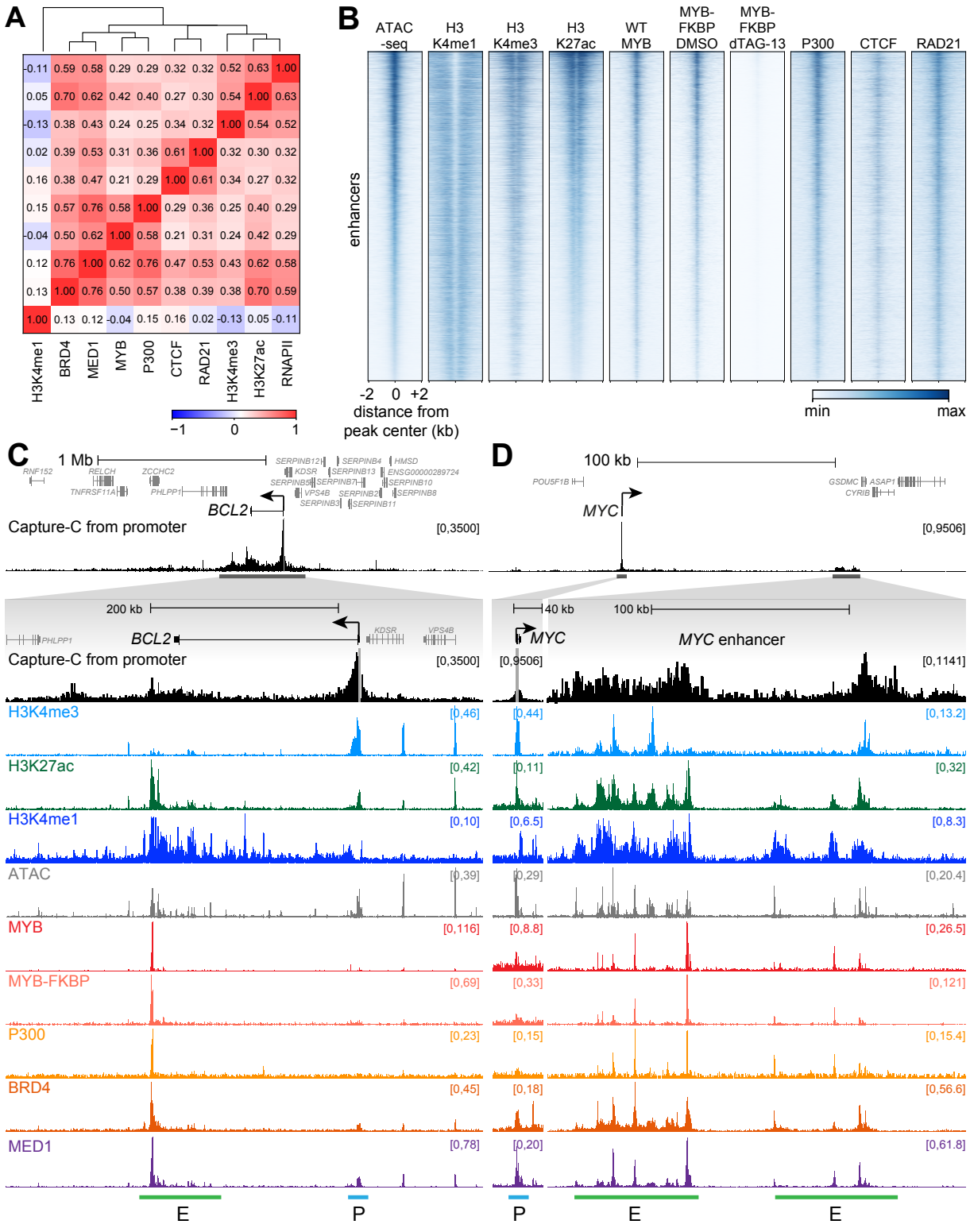
A
H3K4me1
BRD4
MED1
MYB
P300
CTCF
RAD21
H3K4me3
H3K27ac
RNAPII
−1
0
1
B
ATAC -seq
H3 K4me1
H3 K4me3
H3 K27ac
WT MYB
MYB-FKBP DMSO
MYB-FKBP dTAG-13
P300
CTCF
RAD21
enhancers
-2 0 +2
distance from peak center (kb)
min
max
C
1 Mb
BCL2
Capture-C from promoter
[0,3500]
200 kb
H3K4me3
[0,46]
H3K27ac
[0,42]
H3K4me1
[0,10]
ATAC
[0,39]
MYB
[0,116]
MYB-FKBP
[0,69]
P300
[0,23]
BRD4
[0,45]
MED1
[0,78]
E
P
D
100 kb
MYC
[0,9506]
40 kb
MYC enhancer
[0,1141]
[0,44]
[0,13.2]
[0,11]
[0,32]
[0,6.5]
[0,8.3]
[0,29]
[0,20.4]
[0,8.8]
[0,26.5]
[0,33]
[0,121]
[0,15]
[0,15.4]
[0,18]
[0,56.6]
[0,20]
[0,61.8]
P
E
E

Figure 2

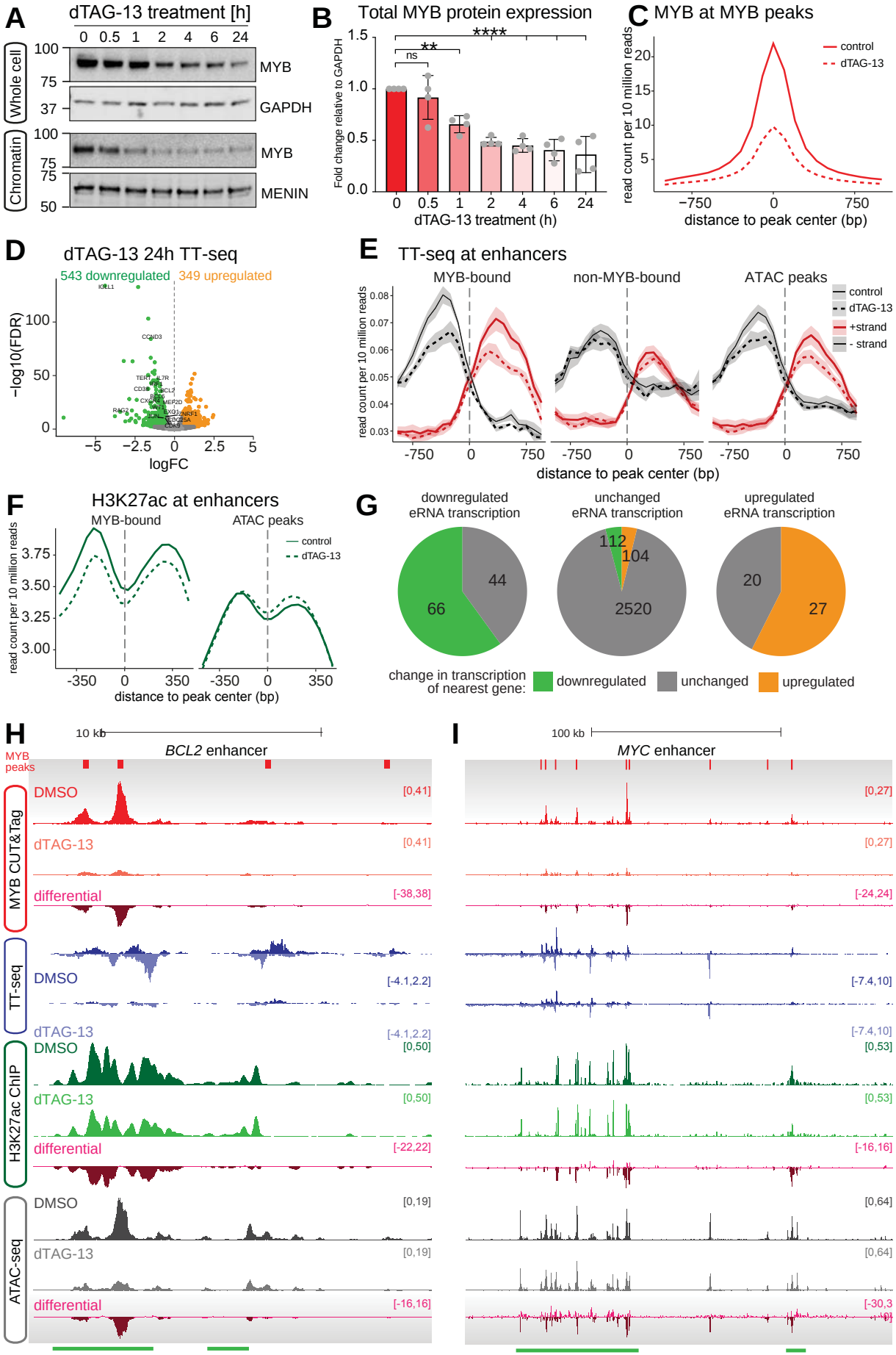
A
dTAG-13 treatment [h]
0 0.5 1 2 4 6 24
Whole cell
Chromatin
MYB
GAPDH
MENIN
B
Total MYB protein expression
Fold change relative to GAPDH
dTAG-13 treatment (h)
C
MYB at MYB peaks
read count per 10 million reads
control
dTAG-13
distance to peak center (bp)
D
dTAG-13 24h TT-seq
543 downregulated
349 upregulated
−log10(FDR)
logFC
E
TT-seq at enhancers
MYB-bound
non-MYB-bound
ATAC peaks
+strand
- strand
F
H3K27ac at enhancers
G
downregulated eRNA transcription
unchanged eRNA transcription
upregulated eRNA transcription
change in transcription of nearest gene:
H
BCL2 enhancer
MYB peaks
MYB CUT&Tag
TT-seq
H3K27ac ChIP
ATAC-seq
I
MYC enhancer

Figure 3

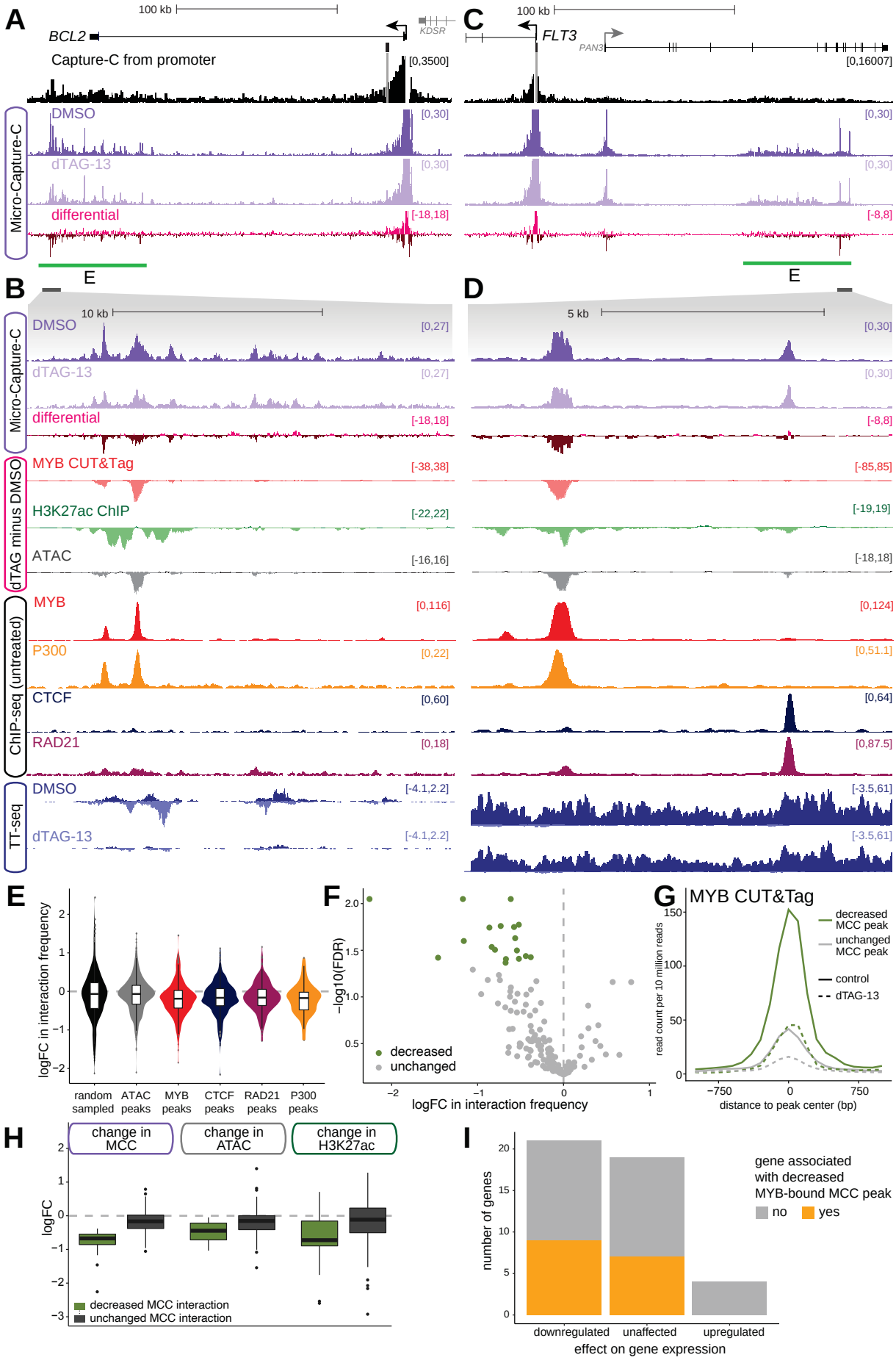
A
100 kb
BCL2
KDSR
Capture-C from promoter
[0,3500]
Micro-Capture-C
DMSO
[0,30]
dTAG-13
[0,30]
differential
[-18,18]
E
C
100 kb
FLT3
PAN3
[0,16007]
[0,30]
[0,30]
[-8,8]
E
B
10 kb
Micro-Capture-C
DMSO
[0,27]
dTAG-13
[0,27]
differential
[-18,18]
dTAG minus DMSO
MYB CUT&Tag
[-38,38]
H3K27ac ChIP
[-22,22]
ATAC
[-16,16]
ChIP-seq (untreated)
MYB
[0,116]
P300
[0,22]
CTCF
[0,60]
RAD21
[0,18]
TT-seq
DMSO
[-4.1,2.2]
dTAG-13
[-4.1,2.2]
D
5 kb
[0,30]
[0,30]
[-8,8]
[-85,85]
[-19,19]
[-18,18]
[0,124]
[0,51.1]
[0,64]
[0,87.5]
[-3.5,61]
[-3.5,61]
E
logFC in interaction frequency
random sampled
ATAC peaks
MYB peaks
CTCF peaks
RAD21 peaks
P300 peaks
F
−log10(FDR)
decreased
unchanged
logFC in interaction frequency
G
MYB CUT&Tag
read count per 10 million reads
decreased MCC peak
unchanged MCC peak
control
dTAG-13
distance to peak center (bp)
H
change in MCC
change in ATAC
change in H3K27ac
logFC
decreased MCC interaction
unchanged MCC interaction
I
number of genes
gene associated with decreased MYB-bound MCC peak
no
yes
downregulated
unaffected
upregulated
effect on gene expression

Figure 4

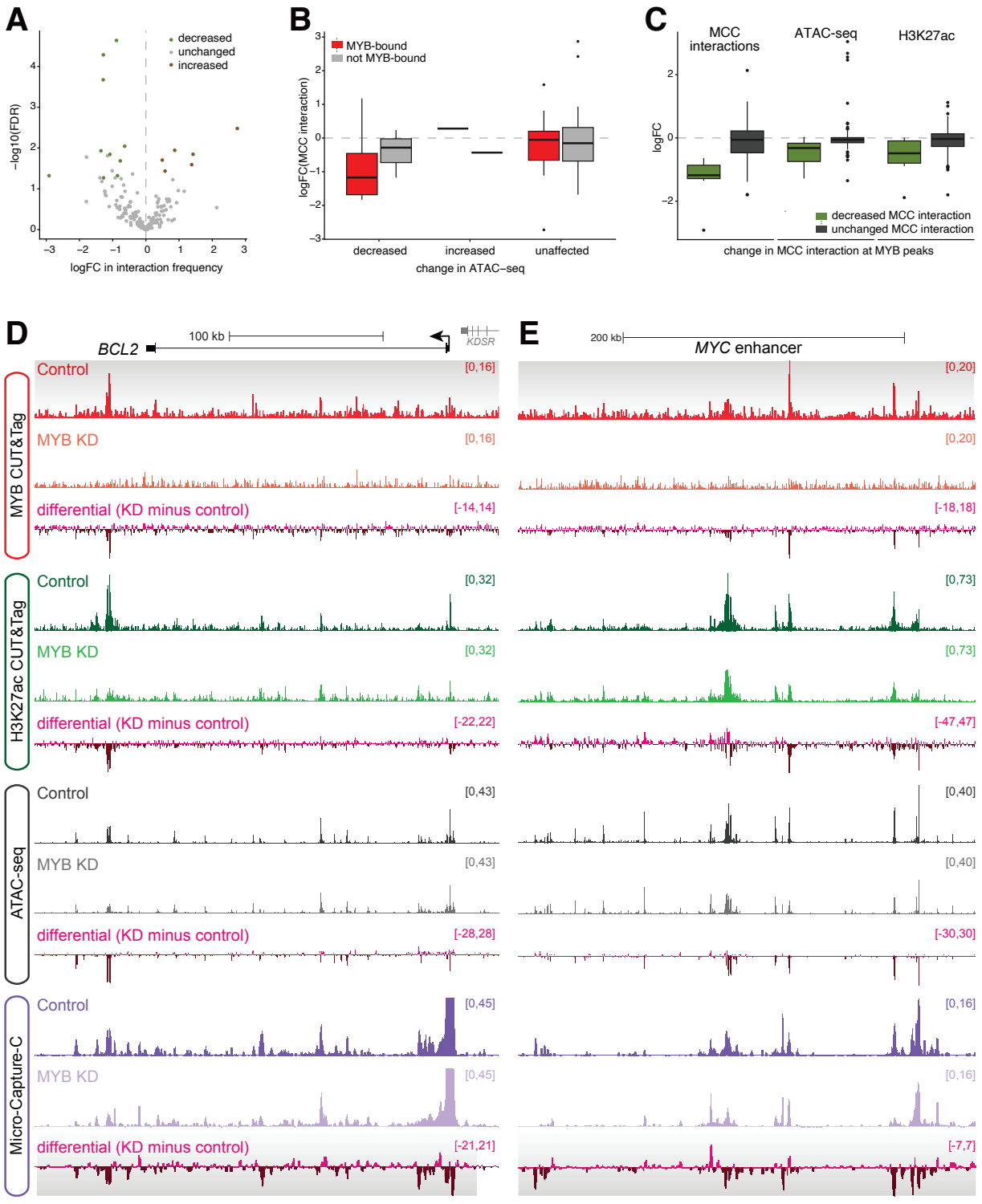
A
decreased
unchanged
increased
−log10(FDR)
logFC in interaction frequency
B
MYB-bound
not MYB-bound
logFC(MCC interaction)
decreased
increased
unaffected
change in ATAC−seq
C
MCC interactions
ATAC-seq
H3K27ac
logFC
decreased MCC interaction
unchanged MCC interaction
change in MCC interaction at MYB peaks
D
BCL2
100 kb
KDSR
MYB CUT&Tag
Control
[0,16]
MYB KD
[0,16]
differential (KD minus control)
[-14,14]
H3K27ac CUT&Tag
Control
[0,32]
MYB KD
[0,32]
differential (KD minus control)
[-22,22]
ATAC-seq
Control
[0,43]
MYB KD
[0,43]
differential (KD minus control)
[-28,28]
Micro-Capture-C
Control
[0,45]
MYB KD
[0,45]
differential (KD minus control)
[-21,21]
E
200 kb
MYC enhancer
[0,20]
[0,20]
[-18,18]
[0,73]
[0,73]
[-47,47]
[0,40]
[0,40]
[-30,30]
[0,16]
[0,16]
[-7,7]

Figure 5

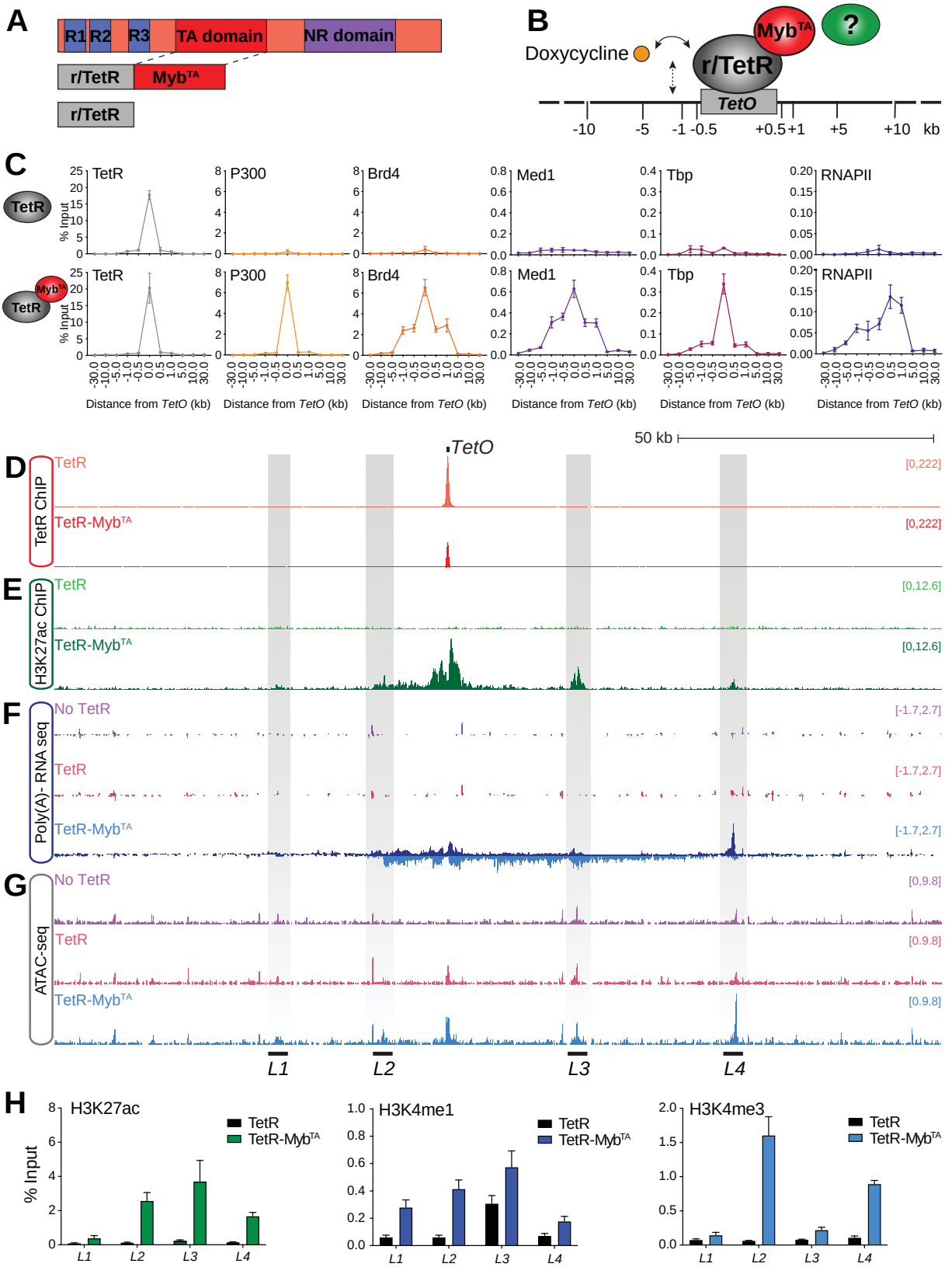
A
R1
R2
R3
TA domain
NR domain
r/TetR
Myb^TA
r/TetR
B
Doxycycline
Myb^TA
?
r/TetR
TetO
-10
-5
-1
-0.5
+0.5
+1
+5
+10
kb
C
TetR
TetR
Myb^TA
TetR
% Input
TetR
P300
Brd4
Med1
Tbp
RNAPII
Distance from TetO (kb)
D
TetR ChIP
TetO
50 kb
TetR
TetR-Myb^TA
[0,222]
[0,222]
E
H3K27ac ChIP
TetR
TetR-Myb^TA
[0,12.6]
[0,12.6]
F
Poly(A)- RNA seq
No TetR
TetR
TetR-Myb^TA
[-1.7,2.7]
[-1.7,2.7]
[-1.7,2.7]
G
ATAC-seq
No TetR
TetR
TetR-Myb^TA
[0,9.8]
[0.9.8]
[0.9.8]
L1
L2
L3
L4
H
H3K27ac
H3K4me1
H3K4me3
% Input
TetR
TetR-Myb^TA
L1
L2
L3
L4

Figure 6

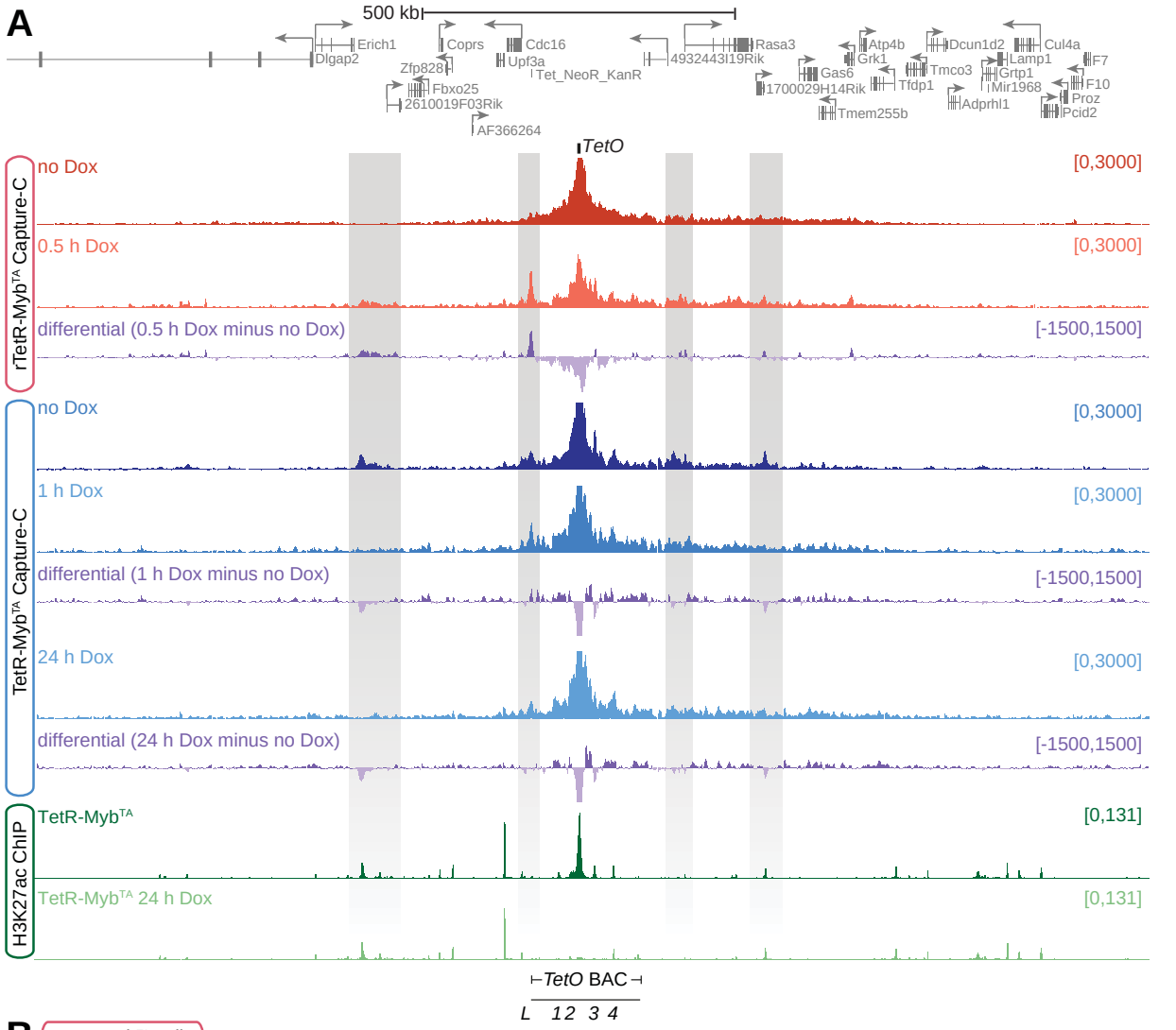
A
500 kb
Erich1
Dlgap2
Coprs
Cdc16
Upf3a
Zfp828
Tet_NeoR_KanR
Rasa3
4932443I19Rik
Atp4b
Grk1
Dcun1d2
Cul4a
Lamp1
F7
Gas6
1700029H14Rik
Tfdp1
Tmco3
Grtp1
Mir1968
F10
Proz
Pcid2
Tmem255b
Adprhl1
Fbxo25
2610019F03Rik
AF366264
TetO
rTetR-MybTA Capture-C
no Dox
[0,3000]
0.5 h Dox
[0,3000]
differential (0.5 h Dox minus no Dox)
[-1500,1500]
TetR-MybTA Capture-C
no Dox
[0,3000]
1 h Dox
[0,3000]
differential (1 h Dox minus no Dox)
[-1500,1500]
24 h Dox
[0,3000]
differential (24 h Dox minus no Dox)
[-1500,1500]
H3K27ac ChIP
TetR-MybTA
[0,131]
TetR-MybTA 24 h Dox
[0,131]
TetO BAC
L 1 2 3 4
B
rTetR-MybTA cells
TetR
% Input
Distance from TetO (kb)
H3K27ac
% Input
Distance from TetO (kb)
Total RNA
Relative to Gapdh
no Dox
0.5 h Dox
24 h Dox
Distance from TetO (kb)
Total RNA
Fold change rel. to no Dox
no Dox
0.5 h Dox
24 h Dox
L1 L2 L3 L4
C
TetR-MybTA cells
TetR
% Input
Distance from TetO (kb)
H3K27ac
% Input
Distance from TetO (kb)
Total RNA
Relative to Gapdh
no Dox
1 h Dox
Distance from TetO (kb)
Total RNA
Fold change rel. to no Dox
no Dox
1 h Dox
L1 L2 L3 L4
D
H3K27ac ChIP
% Input
Distance from TetO (kb)
Total RNA
Relative to Rn18s (10-4)
Distance from TetO (kb)
Total RNA
Relative to Rn18s (10-5)
Distance from TetO (kb)
Total RNA
Fold change rel. to Rn18s
TetR-MybTA
TetR-MybTA M303V
TetR-MybTA L302A
L1 L2 L3 L4

Investigating the role of MYB in enhancer activation and directing 3D chromatin interactions in leukemia

Context of Research

MYB is a key hematopoietic transcription factor that is frequently deregulated in leukemia. The exact mechanism by which it upregulates oncogenic transcription is unknown.

Aim of This Study

To understand how MYB activates oncogenic enhancers to maintain gene expression and promote leukemia

Findings

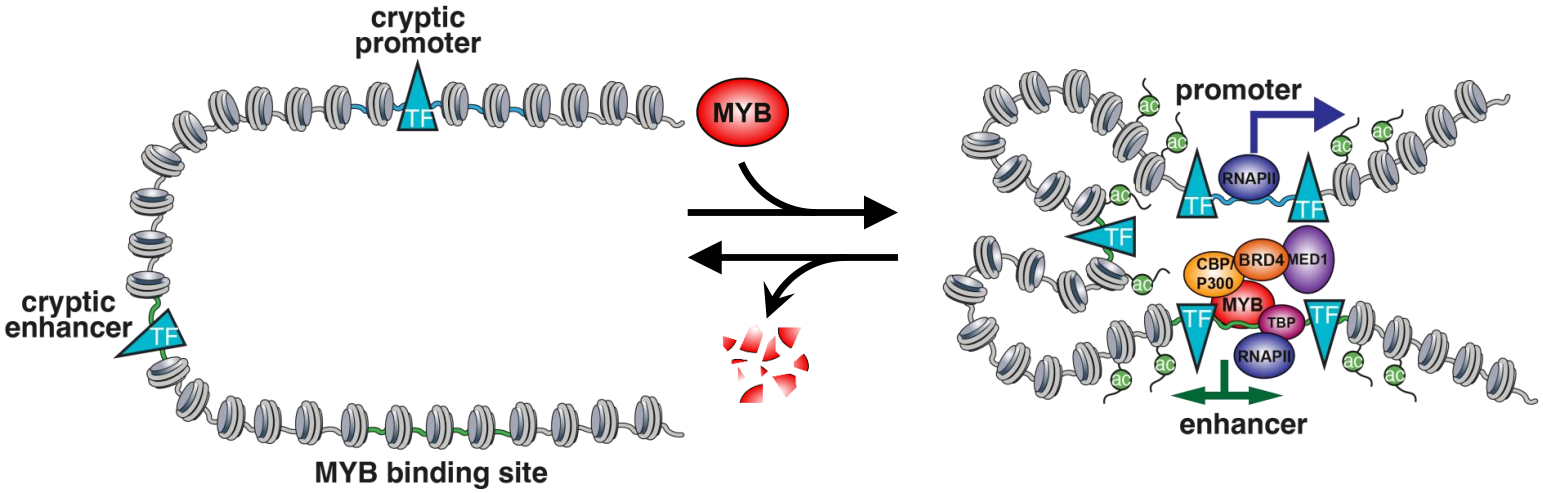

Conclusions: **MYB binding is sufficient to drive novel enhancer activation, including initiating 3D contact with target promoters to drive expression of distal oncogenes. Continued MYB binding is required to maintain enhancer-promoter interactions.**

*Lau et al. DOI: 10.xxxx/**blood**.2026xxxxxx*

Supplemental Methods

Cell culture

SEM cells (DSMZ) were cultured in Iscove's Modified Dulbecco's Medium (IMDM) supplemented with 10% fetal bovine serum (FBS, ThermoFisher Scientific) and 2 mM GlutaMAX (ThermoFisher Scientific). THP-1, RCH-ACV and OCI-AML3 cells (DSMZ) were cultured in RPMI-8226 supplemented with 10% FBS and 2 mM GlutaMAX. Mouse ESCs with a *TetO* array insertion (TOT2N mESC) were the kind gift of Prof. Rob Klose (University of Oxford) and were grown in Dulbecco's Modified Eagle's Medium (DMEM) supplemented with 10% FBS, non-essential amino acids (ThermoFisher Scientific), GlutaMAX, LIF and β-mercaptoethanol. All cell lines were confirmed free from mycoplasma contamination. Colony forming assays were conducted by plating 500 cells mixed with 1 ml H4100 Methylcellulose medium (StemCell Technologies) in a 3 cm diameter dish in triplicate, then allowing to grow for 14 days before counting.

Generation of degron cell lines

SEM cells were edited to incorporate *FKBP12^{F36V}-HA-P2A-mNeonGreen*, immediately prior to the stop codon of both alleles of *MYB*, by CRISPR/Cas9-mediated homology-directed repair (HDR), as previously described.[1] Cells were co-electroporated with pX458 (encoding *Cas9*, one of three sgRNA sequences targeting the end of *MYB* (supplemental Table 2), and *mRuby*) and an HDR construct containing the *FKBP12^{F36V}-HA-P2A-mNeonGreen* sequence flanked by 500 bp regions with homology to either side of the *MYB* stop codon. Fluorescence-activated cell sorting was used to isolate mRuby-positive cells after 24h, and cells were allowed to grow for 1-2 weeks, after which cells were sorted again. mNeonGreen-positive cells were plated onto H4100 Methylcellulose medium and after 1-2 weeks, individual colonies screened for homozygous editing of the *MYB* gene by PCR and western blotting.

TetR cell lines

The Myb transcriptional activation domain (Myb^{TA}) and Myb^{TA} mutant sequences (Myb^{TA} L302A and Myb^{TA} M303V) were cloned into the original pCAGFS2TetR vector, downstream of the FS2-TetR open reading frame. The rTetR-MYB^{TA} construct was generated by dsODN exchange cloning, replacing the TetR domain with the rTetR sequence.[2] Plasmids were transfected into TOT2N mESCs with Lipofectamine-2000, and clones stably expressing the transfected construct were selected using 1 μg/ml puromycin, then confirmed by western blotting. As a negative control, parental mESCs (no TetR) or cells expressing the TetR domain alone were used. Where indicated, cells were treated with 1 μg/ml doxycycline.

siRNA transfections

siRNA knockdown assays were performed using a rectangle pulse EPI 2500 electroporator (Fischer Heidelberg, Germany.[3] 10 µl 10 µM siRNA (ON-TARGETplus Human MYB siRNA L-003910-00-0005 or ON-TARGETplus Non-targeting Control Pool D-001810-10-05) was added to 2 x 10^7 THP-1, OCI-AML3 or RCH-ACV cells resuspended in 800 µl media, and electroporated at 330 V for 0.1 seconds in a 2 mm cuvette. Following electroporation, cells were incubated at room temperature for 10-15 minutes. The cells were then transferred to warm RPMI media (supplemented with 10% FCS and 1% GlutaMax) at a concentration of 1 x 10^6/ml and incubated at 37°C, 5% CO_2. RNA was extracted 24h post-transfection and MYB knockdown confirmed by western blot.

Apoptosis assay

5 x 10^5 SEM-WT or SEM-MYB-FKBP cells were resuspended in FACS buffer (PBS +10% FBS) and placed on Attune NxT analyser. Apoptotic cells were quantified with the eBioscience Annexin V Apoptosis Detection kit (Thermofisher).

Chromatin immunoprecipitation (ChIP)

ChIP was conducted as described previously.[4,5] Briefly, 10^7 cells were fixed for histone modifications (1% formaldehyde for 10 min) or TFs/cofactors (2 mM disuccinimidyl glutarate for 30 min, then 1% formaldehyde for 30 min). Fixed cell pellets were lysed in 120 µl lysis buffer (10 mM Tris-HCl pH 8.0, 1 mM EDTA, 1% SDS) and sonicated with an ME220 sonicator (Covaris) to generate 200-300 bp fragments. After pelleting insoluble material, the supernatant was diluted 10x, then 5 µl protein A- and G-coupled dynabeads (ThermoFisher Scientific) were added to pre-clear chromatin prior to immunoprecipitation. An input sample was taken, then 2 µg antibody (supplemental Table 3) was added and the sample was incubated overnight with rotation at 4 ˚C. Antibody-chromatin complexes were isolated by addition of 15 µl protein A- and G-coupled dynabeads, after which the beads were washed 3x with RIPA buffer (50mM HEPES-KOH (pH 7.6), 500mM LiCl, 1mM EDTA, 1% NP40 and 0.7% sodium deoxycholate) and once with Tris-EDTA. Samples were eluted with lysis buffer, then RNase A- and proteinase K-treated and crosslinks were reversed by overnight incubation at 65 ˚C. DNA was purified using the QIAquick PCR Purification Kit (Qiagen) and quantified by qPCR, normalized to input. Primer sequences are detailed in supplemental Table 2. ChIP-seq libraries were generated with the NEBNext Ultra II DNA library prep kit (NEB), then sequenced by 75 cycle paired-end sequencing on a NextSeq machine (Illumina). All datasets used are reported in supplemental Table 4.

TOPmentation

TOPmentation was conducted as previously described.[6] Briefly, protein A-coupled magnetic beads were pre-incubated with anti-HA antibody (3724S, Cell Signaling Technology) for 4 h with rotation at 4 ˚C. 2.5x10^5 cells were fixed (2 mM disuccinimidyl glutarate for 30 min, then 1% formaldehyde for 30 min), lysed in TOPmentation lysis buffer (50 mM Tris-HCl pH 8.0, 0.5%

SDS, 10 mM EDTA, 1x protease inhibitor cocktail), then sonicated with an ME220 sonicator (Covaris) as for ChIP. Sonicated chromatin was incubated with Triton-X100 (final concentration 1%) for 10 min at room temperature to neutralize the SDS, then pre-cleared with 5 µl protein A-coupled beads. Antibody-incubated beads were washed in PBS/0.5% FBS, then the pre-cleared chromatin was added to the antibody-bound beads and incubated with rotation overnight at 4 ˚C.

The chromatin/antibody-bound beads were transferred to fresh tubes, and washed three times with RIPA buffer (see ChIP protocol), then once with Tris-EDTA and finally with 10 mM Tris-HCl pH8.0. The chromatin was then tagmented by resuspension in 29 µl Tagmentation buffer (10 mM Tris-HCl pH 8.0, 5 mM $MgCl_2$, 10% dimethylformamide) and addition of 1 µl Tn5 transposase (Illumina), then incubation at 37 ˚C for 10 min. The reaction was stopped by addition of 150 µl RIPA buffer, then beads were washed once with 10 mM Tris-HCl pH8.0 and resuspended in 22.5 µl H_2O. Samples were indexed by addition of Nextera indexing primers[7] to 125 nM final concentration) 25 µl NEBNext Ultra II Q5 MasterMix (NEB). Libraries were amplified using the following thermal profile: 72 ˚C 5 min, 95 ˚C 5 min, (98 ˚C 10 s, 63 ˚C 30 s, 72 ˚C 3 min) x 11 cycles, then clean-up was performed using a 1:1 ratio of Agencourt AMPure XP beads. Samples were sequenced by 75 cycle paired-end sequencing on a NextSeq machine (Illumina).

CUT&Tag (TF-optimised)

Cell were resuspended in NE1 buffer (20 mM HEPES KOH pH 7.9, 10 mM KCl, 0.5 mM spermidine, 0.1% Triton X-100, 20% glycerol, 1× Complete Protease Inhibitor [EDTA-free]) followed by 10 min incubation on ice. Nuclei were pelleted at 500g for 10 mins at 4°C then fixed in 0.1% Formaldehyde for 2 min. Nuclei were quenched with 1.25 M Glycine then pelleted at 500g for 10 min at 4°C followed by resuspension in wash buffer (25mM HEPES-KOH, 110mM KCl, 10mM NaCl, 1mM $MgCl_2$, 1% (w/v) BSA, 0.5 mM Spermidine, 1x Complete Protease Inhibitor [EDTA-free]). Concanavalin A (Con A) beads were activated by washing (2x) with 1 ml Concanavalin Activation Buffer (20 mM HEPES-KOH pH 7.9, 10 mM KCl, 1 mM $CaCl_2$, 1 mM $MnCl_2$). For each antibody/sample combination, 5 µl of activated ConA beads were added to 5 x 10^4 nuclei. Nuclei were incubated with 0.5 µl of primary antibody in 25 µl of antibody buffer (0.1% BSA, 2 mM EDTA in Wash Buffer) for either 1 h at RT or overnight at 4°C. Nuclei were then incubated with 25µl of 1:100 secondary antibody (Guinea Pig anti-Rabbit IgG) for 30 mins at RT then washed with 200 µl Wash Buffer and incubated with 25 µl 1:20 pAG-Tn5 (EpiCypher) in WB-300 (300 mM NaCl in Wash Buffer) for 1hr at room temperature. Nuclei were washed (x2) with 200 µl of WB-300 to remove unbound pAG-Tn5 and then incubated at 37°C for 1 h in 50µl Tagmentation buffer (10 mM $MgCl_2$ in WB-300). Tagmentation was stopped by washing with 50 µl TAPS Wash Buffer (10 mM TAPS pH 8.5, 0.2 mM EDTA) before lysing the nuclei with 5 µl SDS-ProK Buffer (1% SDS, 10 mM TAPS pH 8.5, Thermolabile Proteinase K) and incubating for 1 h at 37° C and 1 h at 58°C. SDS was neutralised with 15 µl 6% Triton and tagmented DNA amplified with NEBNext Ultra II Q5 Master Mix and indexed primers (thermal profile: 58 °C

5 min, 72 °C 5 min, 98 °C 5 min, [98 °C 10 sec, 60 °C 10 sec, 72 °C 1 min] ×12). Libraries were cleaned with Agencourt AMPure XP beads and sequenced on NovaSeq X.

ATAC-seq

ATAC-seq was conducted using 50000 live cells using Nextera Tn5 transposase (Illumina) as previously described,[8] and sequenced by 75 cycle paired-end sequencing on a NextSeq machine (Illumina).

ChIP-seq/TOPmentation and ATAC-seq analysis

FASTQ file quality was confirmed by FastQC (v0.12.1; http://www.bioinformatics.babraham.ac.uk/projects/fastqc/), after which reads were trimmed using trim_galore with Cutadapt (v0.6.10; https://www.bioinformatics.babraham.ac.uk/projects/trim_galore/). Trimmed reads were mapped to the hg38 reference genome using Bowtie 2 (v2.5.1).[9] PCR duplicates were removed with picard MarkDuplicates (v3.0.0; http://broadinstitute.github.io/picard). The ENCODE Blacklist (https://doi.org/10.1038/s41598-019-45839-z) was used to remove problematic mapping regions from the aligned files and further QC of the aligned files was performed using samtools (v1.17).[10] For ChIP-seq/TOPmentation/CUT&Tag, peaks were called using the HOMER (v4.11)[11] function findPeaks, providing the input track as background, with the flag –style histone or –style factor as appropriate. For ATAC-seq, peaks were called using MACS2.[12] Bigwigs were generated using HOMER and visualized in the UCSC genome browser.[13] Putative enhancers were identified by the intersection of non-promoter ATAC-seq peaks with H3K27ac peaks, and assigned to the nearest transcriptional start site. Metaplots were generated using the HOMER function annotatePeaks.pl,[11] centered on enhancer ATAC-seq peaks. Heatmaps were generated using deepTools (v3.5.1).[14] Motif analysis was conducted using FIMO (v5.5.3)[15] with the HOCOMOCO v14 core mouse motif database.[16] Only motifs meeting two criteria were included: the transcription factor is expressed (CPM > 5 from RNA-seq) and the motif match was $q < 0.05$. Gene ontology analysis was conducted using gprofiler2.[17]

Transient Transcriptome sequencing (TT-seq)

TT-seq was conducted as previously described.[18] Briefly, spike-in RNA was generated by in vitro transcription of exogenous plasmid sequences in the presence of 4S-UTP (Jena Bioscience), using the MEGAscript kit (ThermoFisher Scientific). $5x10^7$ SEM cells were treated with 500 μM 4-thiouridine (Abcam) for 5 min, before RNA isolation by Trizol extraction (ThermoFisher Scientific) with the addition of 60 ng spike-in RNA, then DNase I-treatment. Labelled nascent RNA was fragmented briefly by sonication (Covaris), biotinylated with EZ-link biotin-HPDP (ThermoFisher Scientific), then purified by streptavidin bead pull-down (Miltenyi). Strand-specific libraries were prepared using the NEBNext Ultra II Directional RNA Library Prep Kit for

Illumina (NEB) and sequenced by 150 cycle paired-end sequencing on a NextSeq machine (Illumina).

Nascent RNA sequencing

5×10^7 cells were treated with 500 μM 4-thiouridine (Abcam) for 1 h. Cells were lysed with TRIzol (Thermo Fisher Scientific) and total RNA was extracted with chloroform and precipitated with ethanol. Following DNase treatment with TURBO DNA-free Kit (ThermoFisher Scientific) as per the manufacturer's instructions, labelled nascent RNA was biotinylated by labelling with 1 mg/ml Biotin-HPDP (ThermoFisher Scientific) for 90 min at room temperature. Following chloroform extraction, labelled RNA was separated using magnetic streptavidin beads (Miltenyi). Beads were washed using a magnetic μMACS stand before RNA was eluted in two rounds of elution with 100 μl 100 mM DTT. RNA was purified using a QIAGEN RNeasy MinElute Cleanup Kit. Libraries were prepared using the NEBNext Ultra Directional RNA Library Preparation Kit for Illumina (New England Biolabs). Libraries were sequenced paired-end on a NextSeq 500 (Illumina) using a NextSeq® High Output v2 150 cycle sequencing kit.

PolyA-minus RNA sequencing

RNA was extracted from cells using the RNeasy Mini Kit (Qiagen). PolyA-minus RNA was isolated using the NEBNext Poly(A) mRNA magnetic isolation module (retaining the unbound fraction), then used to generate a strand-specific library using the NEBNext Ultra II Directional RNA Library Prep Kit for Illumina (NEB). Libraries were sequenced by 150 cycle paired-end sequencing on a NextSeq machine (Illumina).

RNA-seq analysis

Reads were subjected to quality checking by fastQC (v0.12.1) and trimming using trim_galore (v0.6.10) to remove contaminating sequencing adapters, poor quality reads and reads shorter than 21 bp. Reads were then aligned to hg38 using STAR (v2.4.2a)[19] in paired-end mode using default parameters. Gene expression levels were quantified as read counts using the featureCounts function from the Subread package (v2.0.2)[20] with default parameters. The read counts were used to identify differential gene expression between conditions using the EdgeR (v3.12)[21] package. For TT-seq, spike-in RNA levels were quantified by mapping to a custom genome using featureCounts and used to normalize the output of EdgeR. Differential eRNA expression was conducted by counting TT-seq reads at intergenic enhancer ATAC peaks, counting 1 kb upstream on the negative strand and 1 kb downstream on the positive strand. Differential analysis was conducted using EdgeR.

qRT-PCR

RNA was extracted from cells using the RNeasy Mini Kit (Qiagen), then reverse transcribed using SuperScript III (ThermoFisher Scientific) with random hexamer primers. cDNA was analyzed by qPCR using Taqman probes (ThermoFisher Scientific) or SyBr Green (ThermoFisher Scientific). The housekeeping genes *GAPDH* and *YWHAZ* were used for normalization. Taqman probe IDs and SyBr primer sequences are detailed in supplemental Table 2.

Cellular fractionation and western blotting

Cellular fractionation was performed to separate cytoplasmic, nucleoplasmic, and chromatin-associated proteins from SEM cells. Briefly, 1×10^7 cells were lysed on ice in Buffer A (10 mM HEPES pH 7.9, 10 mM KCl, 1.5 mM $MgCl_2$, 0.34 M sucrose, 10% glycerol, 0.2% NP-40, supplemented with DTT and protease inhibitors) to release the cytoplasmic fraction, and intact nuclei were pelleted by low-speed centrifugation. Nuclei were washed and resuspended at in no-salt buffer (3 mM EDTA, 0.2 mM EGTA, protease inhibitors) to extract the soluble nucleoplasmic fraction, leaving a chromatin-enriched pellet. Chromatin-associated proteins were recovered by high-salt extraction using BC-300 buffer (50 mM Tris-HCl pH 8.0, 300 mM KCl, 5 mM EDTA, 20% glycerol, 0.5% NP-40, supplemented with benzonase and protease inhibitors). All fractions were normalized to equivalent cell numbers, mixed with SDS loading buffer, boiled, and analyzed by SDS–PAGE and western blotting. See supplemental Table 3 for antibody details.

Next Generation Capture-C

Capture-C was conducted as described previously,[22,23] using $2x10^7$ cells per replicate. Briefly, DpnII-generated 3C libraries were sonicated to 200 bp fragments and Illumina paired-end sequencing adaptors (New England Biolabs) were added using Herculase II (Agilent). Indexing was performed in duplicate to maintain library complexity, with libraries pooled after indexing. Enrichment was performed using biotinylated Capture-C probes (supplemental Table 1),[4] with two successive rounds of hybridization, streptavidin bead pulldown (ThermoFisher Scientific), bead washes and PCR amplification using the HyperCapture Target Enrichment Kit (Roche). Samples were sequenced by paired-end sequencing with a 300 cycle high-output Nextseq 500 kit (Illumina). Data analysis was performed using CapCruncher v0.2.0[22] (https://doi.org/10.5281/zenodo.6326102) and statistical analysis was performed as described.[22,23]

Micro-Capture-C

Micro-Capture-C was performed as described.[24,25] Briefly, 10^7 SEM cells were fixed with 2% formaldehyde for 10 min, then quenched with glycine and PBS-washed. After permeabilization with 0.005% digitonin for 15 min, cells were snap frozen. Thawed cells were pelleted and resuspended in reduced-calcium MNase buffer (10 mM Tris-HCl pH7.5, 1 mM $CaCl_2$), then divided into three aliquots. Cells were titrated with different micrococcal nuclease (NEB) concentrations for 1h at 37 ˚C with shaking at 550 rpm. The reaction was stopped by addition of EGTA to 5 mM, with 200 µl removed to assess digestion. Remaining cells were pelleted and

washed with PBS/EGTA, then cell pellets were resuspended in DNA ligase buffer, supplemented with 400 µM dNTPs and 5 mM EDTA, before addition of DNA Polymerase I large (Klenow) fragment (NEB) to 100 U/µl, T4 polynucleotide kinase (NEB) to 200 U/µl and T4 DNA ligase (Thermo Scientific) to 300 U/µl. The reaction was incubated for 2h at 37 ˚C, then for 8h at 20 ˚C, at 550 rpm, then cooled to 4 ˚C. The digested and ligated chromatin was decrosslinked at 65 ˚C in the presence of proteinase K, then DNA was purified using a DNeasy Blood and Tissue Kit (Qiagen). Digestion and ligation was assessed by D1000 TapeStation (Agilent). Library preparation, indexing and capture were performed as described for NG Capture-C. Probes used for capture are given in supplemental Table 1. MCC analysis was performed using the MCC pipeline [25] (https://github.com/jojdavies/Micro-Capture-C). MCC peaks were called from merged bigwig tracks from each oligo viewpoint using Lanceotron,[26] and were then filtered on peak size, width and distance from the viewpoint. Unique junctions within each peak in the control and treated conditions were counted before normalization, using the total cis-unique ligation junctions for that peak's corresponding viewpoint.[25] Junction counts were compared between conditions using a Student's T-test. MCC peaks included in the analysis were intersected with SEM cell ChIP-seq peaks from in-house datasets using Pybedtools with default parameters. The enrichment score was calculated as the number of statistically skewed MCC peaks with factor bound divided by the total number of MCC peaks used for the analysis.

Supplemental Table 1. Probes used for NG Capture-C and Micro-Capture-C.

Micro-Capture-C				
Gene	**Probe coordinates (hg38)**			
	Chromosome	**Start**	**End**	**Biological relevance**
ABCA2	chr9	137028181	137028301	Lipid transporter. Increased expression of *ABCA2* is associated with resistance to specific chemotherapeutic drugs.
ARID1B	chr6	156777888	156778008	Subunit of SWI/SNF remodelling complex, mutations in *ARID1B* are implicated in several cancers.[27]
ASAP2	chr2	9206597	9206717	Regulates the formation of post-Golgi vesicles and modulates constitutive secretion. KMT2A::AFF1 target.
ASXL1	chr20	32358176	32358296	Transcriptional regulator, mutations occur in AML.[28]
BCL11A	chr2	60553575	60553695	Oncogene often activated via translocations or overexpressed in hematological malignancies like B-cell lymphomas, chronic lymphocytic leukemia (CLL), and ALL. It regulates lymphocyte development and is a potential therapeutic target.
BCL2	chr18	63320079	63320199	Anti-apoptotic gene with clinical relevance as a therapeutic target in leukemia, known MYB target.[29]
BRD4	chr19	15331734	15331854	Epigenetic regulator, therapeutic target in hematological malignancies.[30]
CASP2	chr7	143288166	143288286	Regulator of apoptosis, anti-apoptotic role in AML.
CD38	chr4	15778263	15778383	Transmembrane glycoprotein. Therapeutic target in hematological malignancies.[31]
CDC25A	chr3	48188541	48188661	Protein phosphatase, dephosphorylates CDK1, stimulating its kinase activity
CDK6	chr7	92833904	92834024	Cyclin dependent kinase 6, promotes G1/S progression, Enhancer is bound by KMT2A::AFF1.[6]
CXCR4	chr2	136118153	136118273	GPCR chemokine receptor. High expression of *CXCR4* is an indicator of poor prognosis in AML and ALL.[32]
DNMT3A	chr2	25342503	25342623	DNA methyltransferase, mutations occur in hematological malignancies.[33]
E2F1	chr20	33686567	33686687	Transcription factor that regulates the expression of cell cycle and DNA replication genes.
ERG	chr21	38498481	38498601	ETS transcription factor with a role in B-cell development.
EXO1	chr1	241848109	241848229	5' to 3' exonuclease.
EZH2	chr7	148884312	148884432	Histone-lysine methyltransferase, subunit of PRC2 complex.

FLT3	chr13	28100515	28100635	Receptor Tyrosine kinase, mutations in *FLT3* are found in ~30% AML cases.[34]
FOS	chr14	75278763	75278883	Subunit of the AP-1 transcription factor.
GFI1	chr1	92486129	92486249	Transcriptional repressor essential for hematopoiesis.
GNAQ	chr9	78030959	78031079	Couples cell surface GPCR signals to intracellular pathways.
HIVEP2	chr6	142945207	142945327	Binds to viral promoters.
IDH1	chr2	208255188	208255308	Isocitrate dehydrogenase, mutations occur in AML.[35]
IKZF1	chr7	50304591	50304711	Master hematopoietic transcription factor and tumor suppressor. Deletion/mutations are associated with high-risk B-cell precursor ALL.[36]
JAK2	chr9	4984757	4984877	Tyrosine kinase that plays a central role in cytokine and growth factor signalling.
JMJD1C	chr10	63466011	63466131	Histone lysine demethylase.
JUN	chr1	58784140	58784260	Subunit of AP-1 transcription factor.
KRAS	chr12	25250963	25251083	Small GTPase, mutated in many cancers.
LMO4	chr1	87328384	87328504	Transcription factor, KMT2A::AFF1 target.
MBNL1	chr3	152268761	152268881	Splicing modulator.
MCM3	chr6	52284820	52284940	Required for the initiation of eukaryotic genome replication.
MEF2C	chr5	88883102	88883222	Transcription factor involved in myogenesis, ectopic expression linked to leukemia.[37]
MEF2D	chr1	156500929	156501049	Transcription factor involved in myogenesis. MEF2D fusion proteins contribute to B-ALL pathogenesis.[38]
MEIS1	chr2	66435055	66435175	Transcription factor involved in maintaining leukemia stemness, KMT2A::AFF1 target gene.
MSL3	chrX	11758436	11758556	Component of the MSL histone acetyltransferase complex, mediates H4K16ac.
MYC	chr8	127736137	127736257	Transcription factor involved in the pathogenesis of ALL and AML.[39] *MYC* enhancer is a KMT2A::AFF1 target.[6]
NF1	chr17	31094792	31094912	Functions as a tumor suppressor by negatively regulating oncogenic Ras.
PAX5	chr9	37034294	37034414	Transcription factor, master regulator of B-cell development.
PROM1	chr4	16084086	16084206	Transmembrane glycoprotein, maintains stemness. KMT2A::AFF1 target gene.[40]
PTPN11	chr12	112418930	112419050	Protein tyrosine phosphatase.
RUNX1	chr21	34888697	34888817	Transcription factor involved in hematopoeitic development. KMT2A::AFF1 target.[41]
RUNX2	chr6	45422123	45422243	Transcription factor required for osteoblast differentiation. KMT2A::AFF1 target.

SMAD3	chr15	67065867	67065987	Transcriptional modulator activated by TGF-beta.
SPI1	chr11	47378507	47378627	Hematopoietic transcription factor involved in myeloid and B-cell development.
TAPT1	chr4	16226415	16226535	Role in cilia formation.
TERT	chr5	1295077	1295197	Maintains telomeres.
TP53	chr17	7687509	7687629	Tumor suppressor that induces cell cycle arrest, universally mutated across cancer types.
WT1	chr11	32435548	32435668	Transcription factor, mutated in AML.[42]
ZNRF1	chr16	74998959	74999079	E3 ubiquitin-protein ligase
Next Generation Capture-C				
TetO-F	GATCCTTTCAGAGTTCTGGGGGCAGG GGGAGCAGTCTTAGGACCTTGGGTA GAACCAGGTGCCAAGAAGC			
TetO-R	GATCCTGTCCACCCAATCAGCTTCTC TATCACTGATAGGGACTCTTACCCAG GAGATTTGGTCTTCTCTA			

Supplemental Table 2. Primers and oligonucleotides used in this study.

Experiment	Name	Forward Sequence	Reverse sequence
ChIP-qPCR primers	*BCL2* E *(MYB ChIP)*	GAGCCCTCAACCTTGTGATAG	AAGGTAGCCCTGACCATAGA
	MYC E *(MYB ChIP)*	GCACACAAAGGAGAGGCTATT	CCATGTGGGTCCCTTCATTT
	BCL2 E *(CTCF/RAD21 ChIP)*	TGTTGCCTTTAGGCTGTTCT	TCTCACCTGCTCGCTCTAA
	BCL2 P	GTTCAGGTACTCAGTCATCCAC	GGAGGATTGTGGCCTTCTTT
	CD38	GTGAATCGAGTCTGGGACATT	TCTGACCCACAGGTTTGTATTAG
	CDC25A	CATCGGAGGGCATTGATGTAG	CTACCAGCAACTCTCAATTCGT
	CDK6	CTTTCTGGGCCTGAGGATTC	CCAACGTGGTCAGGTGAG
	CXCR4	GTTCACTGCTCTGGGTATCATC	CCTGGTAGGCTTTAGGGTTTG
	JUN	TTTGACGGTTCAGGCTTCTG	CCATTTGCCTTCTTTCTCCATC
	LMO4	AAATATCAGGAGGCACAGAGTTT	CATCTGCTGGTACTCCGATTAAA
	MYC E1	GCTCAAATTGCCCTAACTTCAC	GGCGACTATGGGATAGCATTTA
	MYC E2	CTGGTCAAGGTCTCAGAATCAA	AGGCAGATGCAGGACAATC
	MYC E3	TCTTTCCAGAGCAGCATTCC	AGGCAGTAGATGGCAGTAGA
	RUNX1 E1	CCACCTATTGGCCTTCCTTATG	AGTTGAGGCTTTCTCCAAGTC
	RUNX1 E2	CCATTGCTGAACGCATTGT	CGTCCAGAGGTTGGGATTT
	Human negative	GGCTCCTGTAACCAACCACTACC	CCTCTGGGCTGGCTTCATTC
	Gapdh P	AGAGAGGGAGGAGGGGAAATG	AACAGGGAGGAGCAGAGAGCAC
	Oct4 E	GTGGTGTGAGCAAGTAGGTAG	CTGGCTTAGAGTGTGAACCTTAT
	Oct4 P	CAGACTCCATGAGTCACCTTTAC	AGGGTGTCCCTTTCTTGTTTAC
	Sox2 E	GCTTACTGGAACTTTCCCTAGAA	GGAGACCTGCCATCATCAAA
	Mouse negative	TGGCATAGTCCAAGCAGGGATAG	TCAGATGAGAGACCAAGGCAGAG
qRT-PCR Primers	*BCL2*	Taqman probe ID: Hs00608023_m1	
	MYC	Taqman probe ID: Hs0015348_m1	

	LMO4	Taqman probe ID: Hs01086790_m1	
	CDK6	Taqman probe ID: Hs01026371_m1	
	RUNX1	Taqman probe ID: Hs00231079_m1	
	BCL11A	Taqman probe ID: Hs01093197_m1	
	MBNL1	Taqman probe ID: Hs02569862_s1	
	ARID1B	Taqman probe ID: Hs00368175_m1	
	BCL2 intronic	CGATAACGCCTGCCATCTAA	CCACCACATCCTACTGGATTAC
	CDC25 intronic	TTTCGGATTGCTCCGTACTC	GTGCCTAGAAGAGCCTGATTT
	CDK6 intronic	GGGGATCCTGCGACTAAAAT	TGTCAAAACCCCAACTCTGG
	EXO1 intronic	GCCTGAGTGGAGTATGTGTTT	CGGAATCGTCTGCTCTCTTATC
	FLT3 intronic	GACACTTCTGGTGTCTGTGTAG	CCCTAATTCAAGCCCTCGTTAT
	IKZF1 intronic	AGAGGAATTATCCCGGCTTTG	CCTGAGAAGGTTTGGTGACTT
	LMO4 intronic	GTTCGCCTTCTTCTGAGGTATC	GCCTGTATTGTCTTTGTCCTCT
	MYC intronic	AAGGGAGGCGAGGATGTGTCC	GGCTGGGTGCGGAGATTCG
	RUNX1 intronic	CAAAGAGACAACCAGCATCTTTC	AGCTGCGAGAATGCTTAACT
	SPI1 intronic	AAGGCTGACTCCAGAAAGTG	GATCCCTATGTAGCCAACAGTC
CRISPR sgRNA	*MYB* C-term 1	CACCGGTCTCACATGACCAGCGTC	AAACGACGCTGGTCATGTGAGACC
	MYB C-term 2	CACCGGCATTCTCAGCCCGGACGCT	AAACAGCGTCCGGGCTGAGAATGCC
	MYB C-term 3	CACCGGAGAACACTTCAAGTTGACT	AAACAGTCAACTTGAAGTGTTCTCC
Genotyping primers	*MYB* C-term	TGAAGCTGCTTGGAATGGGT	TGGTGCTGCTCTCAACTGTT
***TetO* primers**	*TetO* -30 kb	GCCGAAGGCTTAGTCTTGAA	AATGGCTGAAACCAGAGCAG

(used for ChIP-qPCR and qRT-PCR)	*TetO* -10 kb	GGCAAGGATACAGGGAGTCA	AAGGACCACCTTAGCCAACA
	TetO -5 kb	TTGGACATAGCACTGAGAAAGAAG	TCCAGACAGGGACTTTGAGTG
	TetO -1 kb	TTTTCCTCATGATGGTACATGG	AATTTGTTGTAGGTGCCATTCA
	TetO -0.5 kb	CTTTAGGAGGGGAGCTGCAT	TTGCCAGTTTTAAGAGAATTTGC
	TetO	TGTGGGCAGGTCACAAGTTA	ATCTCATCCCCAATGCTGTC
	TetO +0.5 kb	AAAGGAAAATGAGGGGCCTA	CAGGCAGGTAAACACGATAAGTT
	TetO +1 kb	CAAATCCGTCCTTGATCTTGA	GCAGTAGGATGGGGAGACAG
	TetO +5 kb	AAGCAACTGGTGTTCACT	CAACCAGAACTCTCCAATACT
	TetO +10 kb	TTCTTCCAAGGCCCTAACCT	CAAGGCAACGTCAAACAATG
	TetO +30 kb	AATGGGAGGCCACCTACAG	TCCGAAGGCCTCAAATGAT
	L1	CCTGTCGGGAAACTGATTTGA	CACTGGAACTGTAGGATTGAGG
	L2	AAGCAGGAACAGAAGGATACG	AGAGCTTCCCACTGGATTTG
	L3	TAGGCACACAGAATGCAAGAG	GCTCAGAAGAAGACAGGAAGATG
	L4	GAGGACACAGATGGAAGAAGAG	ACCAGAGGATCTAGGGAAAGT

Supplemental Table 3. Antibodies used in this study.

Target	Catalogue Number	Company	WB dilution
ACTIN	A4700	Sigma	1:1000
BRD4	A301-985A	Bethyl	
CTCF	3418	Cell Signalling Technology	
FS2 (detects r/TetR)	Gift of Prof Rob Klose (University of Oxford)		
GAPDH	A300-641A	Bethyl	1:10000
H3K4me1	pAb-194-050	Diagenode	
H3K4me3	39159	Active Motif	
H3K27ac	C15410196	Diagenode	
HA (detects MYB-FKBP)	3724S	Cell Signaling Technology	1:5000
MED1	A300-793A	Bethyl	
MENIN	A300-105A	Bethyl	1:10000
MYB	ab109127	Abcam	1:2000
MYBL1	HPA008791	Cambridge Bioscience LtD	1:500
MYBL2	33056T	Cell Signalling Technology	1:500
P300	A300-358A	Bethyl	
RNAPII	sc-899	Santa Cruz	
RAD21	Ab992	Abcam	
TBP	A301-229A	Bethyl	

Supplemental Table 4. Next-Generation Sequencing datasets used in this study.

Cell line	Details	Source
Transient transcriptome-seq		
SEM MYB-FKBP	±dTAG-13 24h	This study
Nascent RNA-seq		
THP-1	±MYB siRNA KD 24h	This study
Poly(A) minus RNA-seq		
mESC No TetR		This study
mESC TetR		This study
mESC TetR-MYB^{TA}		This study
ChIP-seq		
SEM	BRD4	GSE83671
	CTCF	GSE117865
	H3K4me1	GSE74812
	H3K4me3	GSE74812
	H3K27ac	GSE74812
	MED1	GSE83671
	MYB	GSE117865
	P300	GSE85988
	RAD21	GSE139437
	RNAPII	GSE8656968
SEM MYB-FKBP	H3K27ac ±dTAG-13 24h	This study
mESC TetR	TetR (anti-FS2)	This study
	H3K27ac	This study
	Ctcf ±doxycycline 24h	This study
	Rad21 ±doxycycline 24h	This study
mESC TetR-Myb^{TA}	TetR (anti-FS2)	This study
	H3K27ac ±doxycycline 24h	This study
	Ctcf ±doxycycline 24h	This study
	Rad21 ±doxycycline 24h	This study
TOPmentation		
SEM MYB-FKBP	MYB-FKBP (anti-HA)	This study
CUT&Tag		
SEM MYB-FKBP	MYB-FKBP (anti-HA) ±dTAG-13 2h and 24h	This study
SEM MYB-FKBP	MYB-FKBP (anti-HA) ±dTAG-13 2h, then 24h washout	This study
SEM MYB-FKBP	H2K27ac ±dTAG-13 2h and 24h	This study
SEM MYB-FKBP	H2K27ac ±dTAG-13 2h, then 24h washout	This study
OCI-AML3	MYB ±MYB siRNA KD 24h	This study
OCI-AML3	H2K27ac ± MYB siRNA KD 24h	This study
THP-1	MYB ±MYB siRNA KD 24h	This study

THP-1	H2K27ac ± MYB siRNA KD 24h	This study
RCH-ACV	MYB ±MYB siRNA KD 24h	This study
RCH-ACV	H2K27ac ± MYB siRNA KD 24h	This study
ATAC-seq		
SEM		GSE117863
SEM MYB-FKBP ±dTAG-13 24h		This study
OCI-AML3 ±MYB siRNA KD 24h		This study
mESC No TetR		This study
mESC TetR		This study
mESC TetR-Myb^{TA}		This study
Micro-Capture-C		
SEM MYB-FKBP	±dTAG-13 2h and 24h	This study
SEM MYB-FKBP	H2K27ac ±dTAG-13 2h, then 24h washout	This study
OCI-AML3	MYB ±MYB siRNA KD	This study
Next Generation Capture-C		
SEM		GSE117865
mESC TetR-Myb^{TA}	±doxycycline 1h & 24h	This study
mESC rTetR-Myb^{TA}	±doxycycline 0.5h	This study

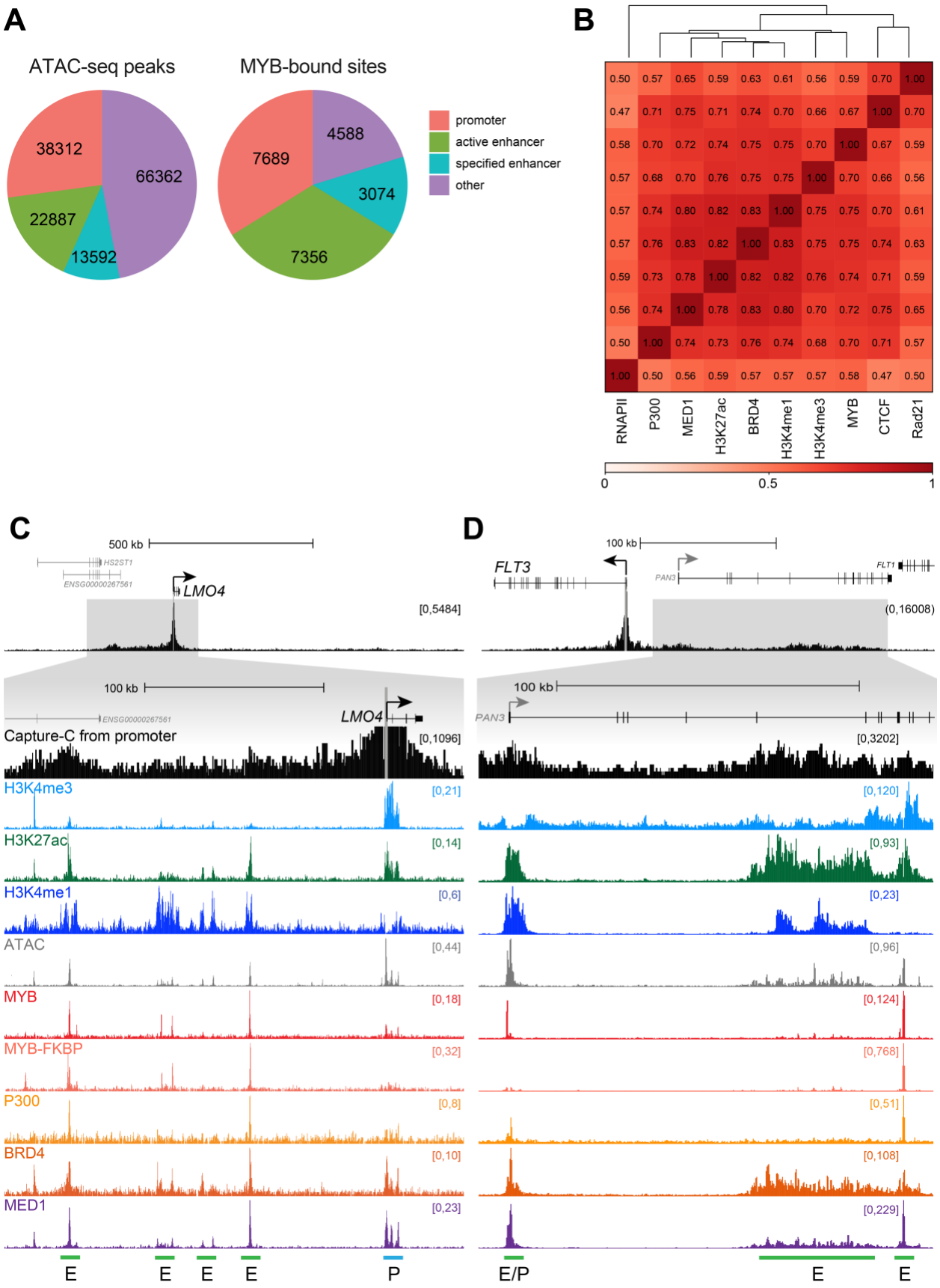
A
ATAC-seq peaks
MYB-bound sites
38312
66362
22887
13592
7689
4588
3074
7356
promoter
active enhancer
specified enhancer
other
B
RNAPII
P300
MED1
H3K27ac
BRD4
H3K4me1
H3K4me3
MYB
CTCF
Rad21
0
0.5
1
C
500 kb
HS2ST1
ENSG00000267561
LMO4
[0,5484]
100 kb
Capture-C from promoter
[0,1096]
H3K4me3
[0,21]
H3K27ac
[0,14]
H3K4me1
[0,6]
ATAC
[0,44]
MYB
[0,18]
MYB-FKBP
[0,32]
P300
[0,8]
BRD4
[0,10]
MED1
[0,23]
E
E
E
E
P
D
100 kb
FLT3
PAN3
FLT1
(0,16008)
[0,3202]
[0,120]
[0,93]
[0,23]
[0,96]
[0,124]
[0,768]
[0,51]
[0,108]
[0,229]
E/P
E
E

Supplemental Figure 1.
(**A**) Proportion of ATAC-seq and MYB peaks overlapping with promoters (within 2 kb of a transcriptional start site [TSS]), active enhancers (H3K27ac peak more than 2 kb from a TSS), specified enhancers (H3K4me1 but no H3K27ac peak, more than 2 kb from a TSS) or other sites. (**B**) Genome-wide Spearman correlation coefficients for ChIP-seq data at ATAC-seq peaks in SEM cells. (**C**) Capture-C, ChIP-seq and ATAC-seq at the *LMO4* gene and enhancer regions (green horizontal lines labelled *E*) in SEM cells. Capture-C was conducted using the promoter (blue horizontal line labelled *P*) as the viewpoint, indicated by the vertical gray bar, mean of three biological replicates. Capture-C traces are scaled to emphasize distal interactions. Upper track shows Capture-C for the broad locus, with an expanded view below. (**D**) Capture-C, ChIP-seq, and ATAC-seq data at *FLT3* as in (B).

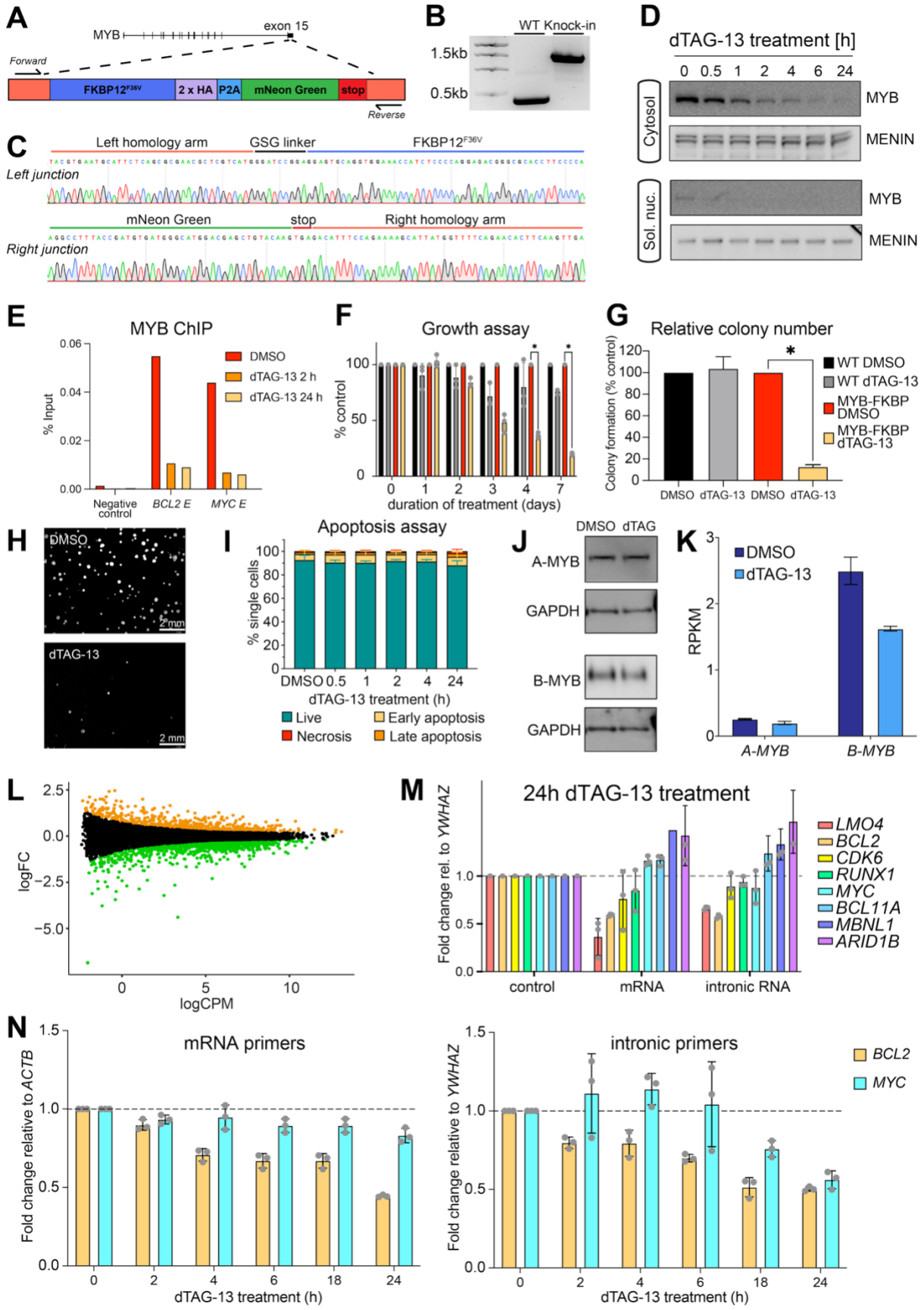
A
MYB
exon 15
Forward
FKBP12F36V
2 x HA
P2A
mNeon Green
stop
Reverse
B
WT Knock-in
1.5kb
0.5kb
C
Left homology arm
GSG linker
FKBP12F36V
Left junction
mNeon Green
stop
Right homology arm
Right junction
D
dTAG-13 treatment [h]
0 0.5 1 2 4 6 24
Cytosol
MYB
MENIN
Sol. nuc.
MYB
MENIN
E
MYB ChIP
% Input
DMSO
dTAG-13 2 h
dTAG-13 24 h
Negative control
BCL2 E
MYC E
F
Growth assay
% control
duration of treatment (days)
G
Relative colony number
Colony formation (% control)
WT DMSO
WT dTAG-13
MYB-FKBP DMSO
MYB-FKBP dTAG-13
DMSO dTAG-13 DMSO dTAG-13
H
DMSO
dTAG-13
2 mm
I
Apoptosis assay
% single cells
DMSO 0.5 1 2 4 24
dTAG-13 treatment (h)
Live
Early apoptosis
Necrosis
Late apoptosis
J
DMSO dTAG
A-MYB
GAPDH
B-MYB
GAPDH
K
DMSO
dTAG-13
RPKM
A-MYB
B-MYB
L
logFC
logCPM
M
24h dTAG-13 treatment
Fold change rel. to YWHAZ
control
mRNA
intronic RNA
LMO4
BCL2
CDK6
RUNX1
MYC
BCL11A
MBNL1
ARID1B
N
mRNA primers
Fold change relative to ACTB
dTAG-13 treatment (h)
intronic primers
Fold change relative to YWHAZ
dTAG-13 treatment (h)
BCL2
MYC

Supplemental Figure 2.
(**A**) Schematic of the FKBP12^{F36V} locus inserted immediately upstream of the stop codon of *MYB*. (**B**) Genomic PCR of the edited locus confirming homozygous insertion of the FKBP12^{F36V} sequence. (**C**) Sanger sequencing traces confirming accurate insertion at the *MYB* locus. (**D**) Western blot for MYB in MYB-FKBP12^{F36V} tagged SEM cells following addition of 0.5 μM dTAG-13. Cells were fractionated, with MENIN used as loading control for the cytosolic and soluble nuclear fractions. Whole cell and chromatin-bound fractions are shown in Figure 2A. (**E**) ChIP-qPCR for MYB in MYB-FKBP12^{F36V} tagged SEM cells following treatment with DMSO or 0.5 μM dTAG-13 for 2 h or 24h. Representative of three biological replicates. (**F**) Growth of untreated (DMSO) or 0.5 μM dTAG-13 treated wild-type and MYB-FKBP12^{F36V} tagged SEM cells over time. Representative of three biological replicates, *$p<0.05$. (**G**) Colony counts 14 days after plating 500 cells per condition (DMSO vs treated with 0.5 μM dTAG-13 for 24h) onto 1 ml of semisolid methylcellulose medium. Data are the mean ± SD of three independent experiments. Three replicates were plated per experiment. (**H**) Representative example of methocellulose assay colonies of MYB-FKBP12^{F36V} tagged SEM cells as in (G). (**I**) Proportion of apoptotic MYB-FKBP12^{F36V} tagged SEM cells following treatment with DMSO or 0.5 μM dTAG-13 for the indicated times. Propidium iodide was used as a live/dead stain, with Annexin V used to identify apoptotic cells by flow cytometry. Data are the mean ± SD of three independent experiments. (**J**) Western blot for A-MYB and B-MYB in MYB-FKBP12^{F36V} tagged SEM cells following addition of 0.5 μM dTAG-13 for 24h. GAPDH is used as a loading control. (**K**) Expression of A-MYB and B-MYB in TT-seq of MYB-FKBP12^{F36V} tagged SEM cells following treatment with DMSO or 0.5 μM dTAG-13 for 24h. Mean of three biological replicates. (**L**) Changes in TT-seq levels following 24h treatment with dTAG-13. Statistically significant differences (green: decreased; orange: increased; black: unchanged) from three biological replicates, FDR < 0.05. (**M**) qRT-PCR analysis of gene expression using mature mRNA and intronic PCR primers following 24h treatment with dTAG-13. Values are normalized *toYWHAZ* mature mRNA levels, relative to DMSO treatment. Mean of three biological replicates; error bars show SEM. (**N**) qRT-PCR analysis of *BCL2* and *MYC* expression following 0.5 μM dTAG-13 treatment for the indicated times, using primers to amplify mature mRNA (left) or intronic RNA (right). Values are normalized to *ACTB* (mature mRNA) or *YWHAZ* (intronic RNA), relative to DMSO treatment. Mean of three biological replicates; error bars show SEM.

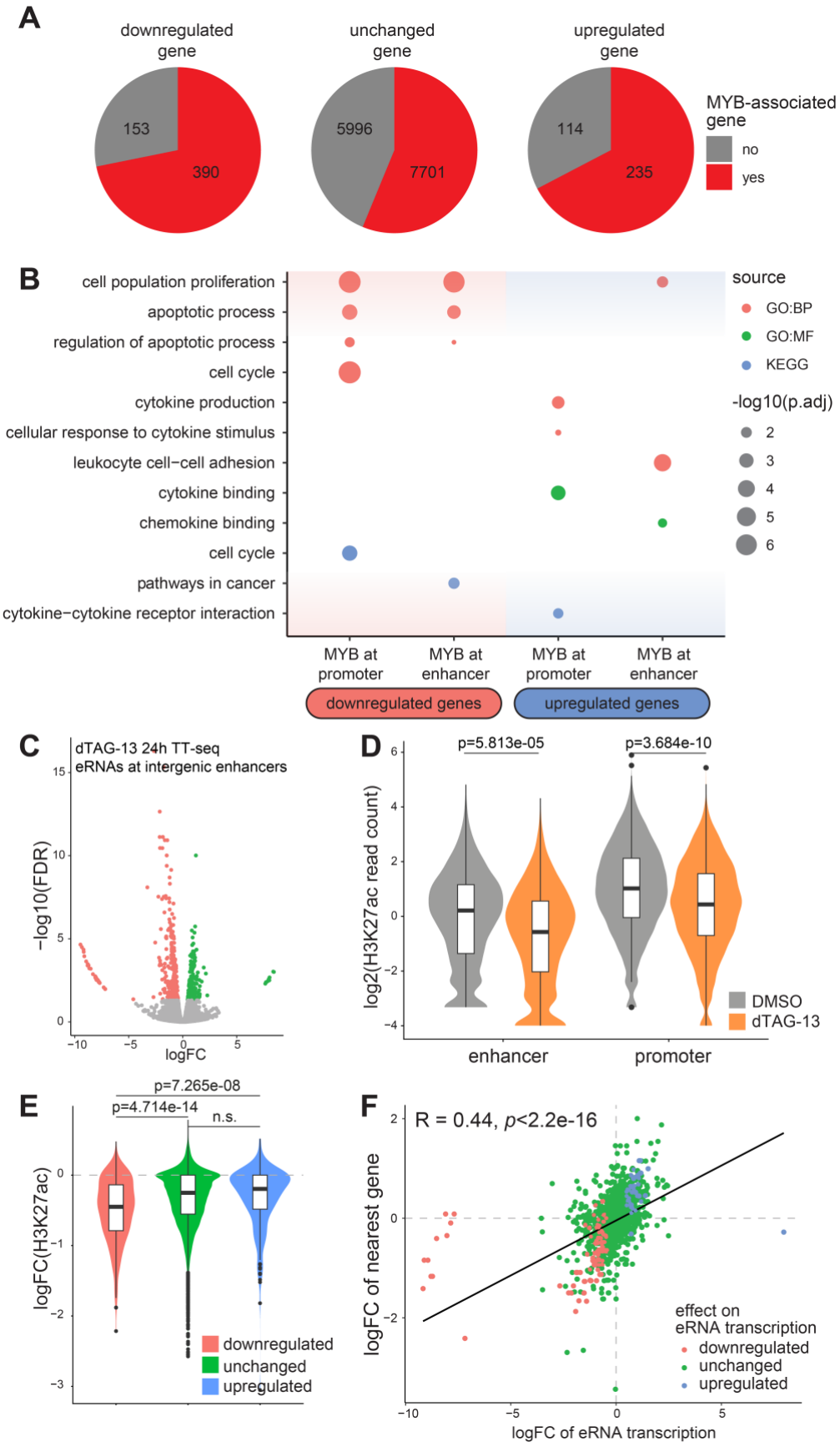
A
downregulated gene
unchanged gene
upregulated gene
153
390
5996
7701
114
235
MYB-associated gene
no
yes
B
cell population proliferation
apoptotic process
regulation of apoptotic process
cell cycle
cytokine production
cellular response to cytokine stimulus
leukocyte cell−cell adhesion
cytokine binding
chemokine binding
cell cycle
pathways in cancer
cytokine−cytokine receptor interaction
source
GO:BP
GO:MF
KEGG
-log10(p.adj)
2
3
4
5
6
MYB at promoter
MYB at enhancer
MYB at promoter
MYB at enhancer
downregulated genes
upregulated genes
C
dTAG-13 24h TT-seq
eRNAs at intergenic enhancers
−log10(FDR)
logFC
D
p=5.813e-05
p=3.684e-10
log2(H3K27ac read count)
DMSO
dTAG-13
enhancer
promoter
E
p=7.265e-08
p=4.714e-14
n.s.
logFC(H3K27ac)
downregulated
unchanged
upregulated
F
R = 0.44, p<2.2e-16
logFC of nearest gene
effect on eRNA transcription
downregulated
unchanged
upregulated
logFC of eRNA transcription

Supplemental Figure 3.
(**A**) Proportion of differentially expressed genes (dTAG-13 24h treatment) associated with MYB binding at the promoter or neighboring enhancer. (**B**) Gene Ontology enrichment of differentially expressed genes associated with MYB binding at the promoter or nearest enhancer. (**C**) Changes in eRNA transcription at intergenic enhancers measured by TT-seq following 24h treatment with dTAG-13 in MYB-FKBP12^{F36V} tagged SEM cells. Statistically significant differences from three biological replicates, FDR < 0.05. (**D**) H3K27ac levels at MYB-bound enhancers and promoters under control conditions and following 24h treatment with dTAG-13. p-values are reported from a Wilcoxon test. (**E**) Change in H3K27ac at intergenic enhancers, separated by the change in eRNA transcription as in C. p-values are reported from a Wilcoxon test. (**F**) Correlation between change in eRNA transcription at intergenic enhancers and change in transcription of the nearest gene. Enhancers are colored by change in eRNA transcription. Spearman correlation coefficient is shown.

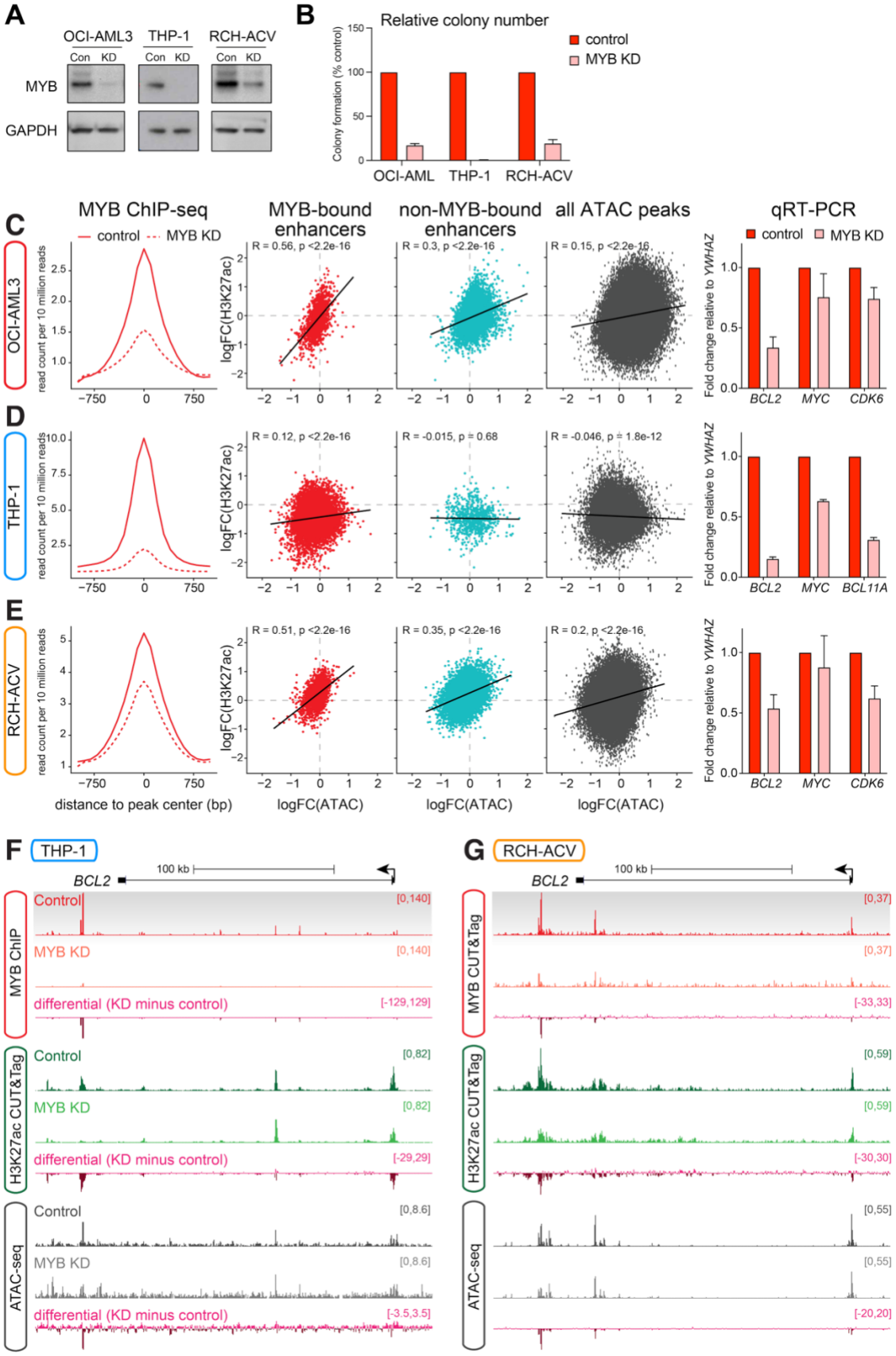
A
OCI-AML3
THP-1
RCH-ACV
Con KD
MYB
GAPDH
B
Relative colony number
control
MYB KD
Colony formation (% control)
OCI-AML
THP-1
RCH-ACV
C
MYB ChIP-seq
MYB-bound enhancers
non-MYB-bound enhancers
all ATAC peaks
qRT-PCR
OCI-AML3
control
MYB KD
read count per 10 million reads
logFC(H3K27ac)
R = 0.56, p <2.2e-16
R = 0.3, p <2.2e-16
R = 0.15, p <2.2e-16
Fold change relative to YWHAZ
BCL2
MYC
CDK6
D
THP-1
R = 0.12, p <2.2e-16
R = -0.015, p = 0.68
R = -0.046, p = 1.8e-12
BCL11A
E
RCH-ACV
R = 0.51, p <2.2e-16
R = 0.35, p <2.2e-16
R = 0.2, p <2.2e-16
distance to peak center (bp)
logFC(ATAC)
F
THP-1
G
RCH-ACV
100 kb
BCL2
MYB ChIP
MYB CUT&Tag
H3K27ac CUT&Tag
ATAC-seq
Control
MYB KD
differential (KD minus control)
[0,140]
[-129,129]
[0,82]
[-29,29]
[0,8.6]
[-3.5,3.5]
[0,37]
[-33,33]
[0,59]
[-30,30]
[0,55]
[-20,20]

Supplemental Figure 4.
(**A**) Western blot for MYB in OCI-AML3, THP-1 and RCH-ACV cells following 24h *MYB* knockdown (KD) or non-targeting control. GAPDH is used as loading control. Representative of three biological replicates. (**B**) Colony counts 14 days after plating 500 OCI-AML3, THP-1 and RCH-ACV cells per condition (NT vs *MYB* KD for 24h) onto 1 ml of semisolid methylcellulose medium. Data are the mean ± SD of three independent experiments. Three replicates were plated per experiment. Analysis of MYB-dependent enhancer activity in OCI-AML3 (**C**), THP-1 (**D**) and RCH-ACV (**E**) cells. Left: Mean MYB CUT&Tag signal at MYB-bound enhancers in control (non-targeting) and 24h *MYB* KD cells. Middle: Correlation between the change in chromatin accessibility (ATAC-seq) and H3K27ac following *MYB* KD at MYB-bound and -unbound enhancers and all ATAC peaks. Right: qRT-PCR analysis of gene expression following *MYB* KD. Values are normalized to *YWHAZ* mature mRNA levels, relative to control treatment. Mean of three biological replicates; error bars show SEM. Spearman correlation coefficients are shown. MYB and H3K27ac ChIP-seq/CUT&Tag and ATAC-seq at *BCL2* in THP-1 (**F**) and RCH-ACV (**G**) cells in control (non-targeting) and 24h MYB KD cells. Differential tracks show the difference between control and KD conditions (KD minus control).

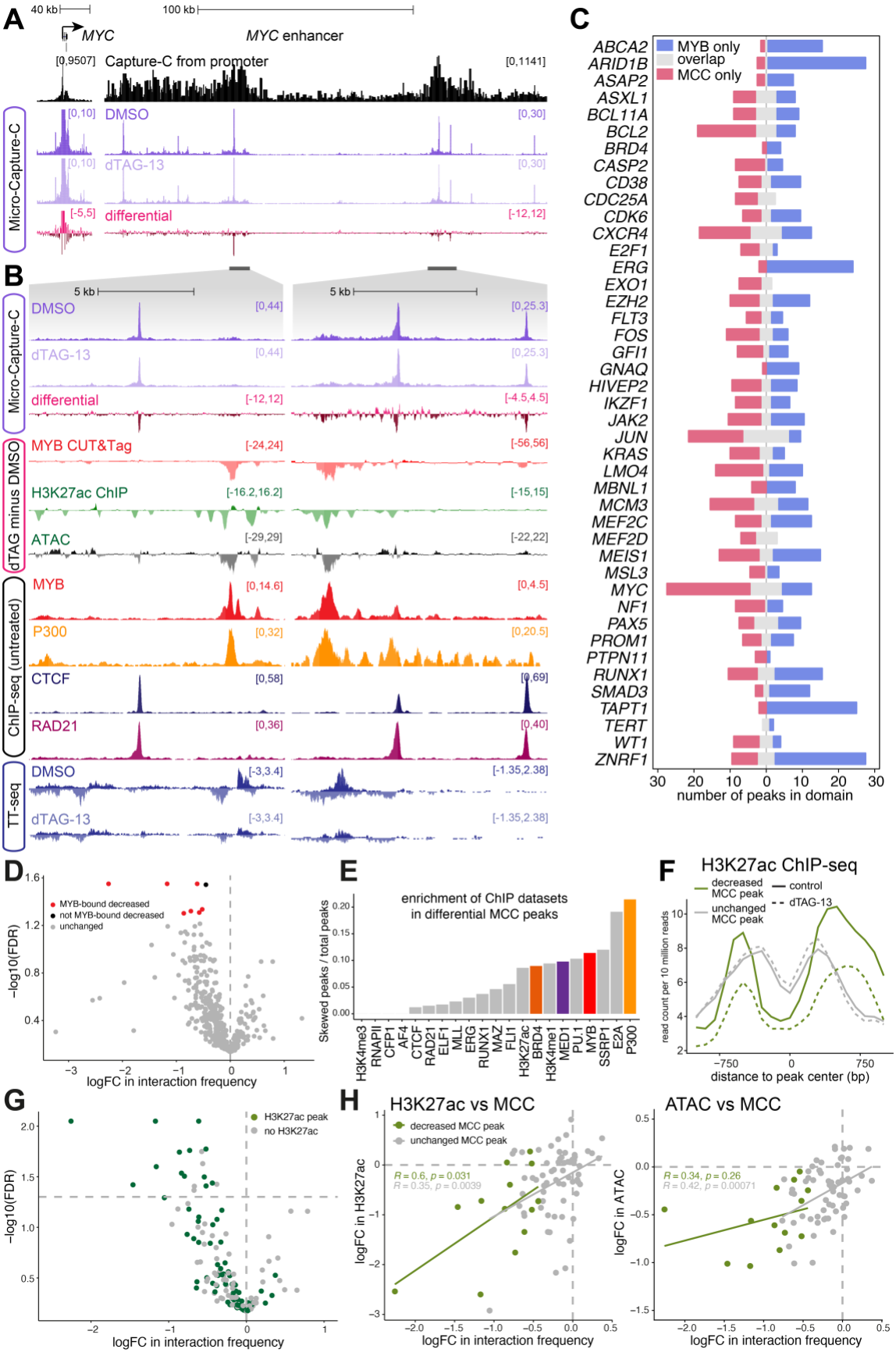
A
40 kb
100 kb
MYC
MYC enhancer
[0,9507]
Capture-C from promoter
[0,1141]
Micro-Capture-C
[0,10]
DMSO
[0,30]
[0,10]
dTAG-13
[0,30]
[-5,5]
differential
[-12,12]
B
5 kb
5 kb
Micro-Capture-C
DMSO
[0,44]
[0,25.3]
dTAG-13
[0,44]
[0,25.3]
differential
[-12,12]
[-4.5,4.5]
dTAG minus DMSO
MYB CUT&Tag
[-24,24]
[-56,56]
H3K27ac ChIP
[-16.2,16.2]
[-15,15]
ATAC
[-29,29]
[-22,22]
ChIP-seq (untreated)
MYB
[0,14.6]
[0,4.5]
P300
[0,32]
[0,20.5]
CTCF
[0,58]
[0,69]
RAD21
[0,36]
[0,40]
TT-seq
DMSO
[-3,3.4]
[-1.35,2.38]
dTAG-13
[-3,3.4]
[-1.35,2.38]
C
MYB only
overlap
MCC only
ABCA2
ARID1B
ASAP2
ASXL1
BCL11A
BCL2
BRD4
CASP2
CD38
CDC25A
CDK6
CXCR4
E2F1
ERG
EXO1
EZH2
FLT3
FOS
GFI1
GNAQ
HIVEP2
IKZF1
JAK2
JUN
KRAS
LMO4
MBNL1
MCM3
MEF2C
MEF2D
MEIS1
MSL3
MYC
NF1
PAX5
PROM1
PTPN11
RUNX1
SMAD3
TAPT1
TERT
WT1
ZNRF1
30 20 10 0 10 20 30
number of peaks in domain
D
MYB-bound decreased
not MYB-bound decreased
unchanged
−log10(FDR)
logFC in interaction frequency
E
enrichment of ChIP datasets
in differential MCC peaks
Skewed peaks / total peaks
H3K4me3
RNAPII
CFP1
AF4
CTCF
RAD21
ELF1
MLL
ERG
RUNX1
MAZ
FLI1
H3K27ac
BRD4
H3K4me1
MED1
PU.1
MYB
SSRP1
E2A
P300
F
H3K27ac ChIP-seq
decreased MCC peak
unchanged MCC peak
control
dTAG-13
read count per 10 million reads
−750
0
750
distance to peak center (bp)
G
H3K27ac peak
no H3K27ac
−log10(FDR)
logFC in interaction frequency
H
H3K27ac vs MCC
decreased MCC peak
unchanged MCC peak
R = 0.6, p = 0.031
R = 0.35, p = 0.0039
logFC in H3K27ac
logFC in interaction frequency
ATAC vs MCC
R = 0.34, p = 0.26
R = 0.42, p = 0.00071
logFC in ATAC
logFC in interaction frequency

Supplemental Figure 5.
(**A**) Capture-C and ChIP-seq in SEM cells, and Micro-Capture-C (MCC), CUT&Tag, ATAC-seq and TT-seq in MYB-FKBP12^{F36V} tagged SEM cells, with or without the addition of dTAG-13 for 24h at the *MYC* locus. (**B**) Enlarged views of regions within the *MYC* enhancer are highlighted by the gray gradient box, and their relative positions within the enhancer annotated by the gray horizontal lines. Capture-C and MCC traces are scaled to emphasize distal interactions. Differential tracks show the difference between DMSO and dTAG-13 conditions (dTAG-13 minus DMSO). (**C**) Overlap of MCC promoter-interacting peaks and MYB peaks within ~500 kb of each gene indicated. (**D**) Change in interaction frequency at all MCC peaks showing interaction with target promoters following 24h treatment with dTAG-13 in MYB-FKBP12^{F36V} tagged SEM cells. Statistically significant differences (red: decreased MYB bound peaks; black: decreased non-MYB-bound peaks; gray: unchanged) from three biological replicates, FDR <0.05. (**E**) Enrichment of SEM ChIP-seq datasets within differential MCC peaks. Statistically significant (FDR <0.05) MCC peaks with ChIP factor bound divided by total number of MCC peaks analyzed with ChIP factor bound. MYB, its interaction partner P300 and enhancer-associated MED1 and BRD4 are highlighted. (**F**) Mean distribution of H3K27ac at MYB-bound MCC interaction peaks in control (untreated) and 24h dTAG-13-treated MYB-FKBP12^{F36V} tagged SEM cells. (**G**) Change in interaction frequency at all MCC peaks bound by MYB, following 24h treatment with dTAG-13 in MYB-FKBP12^{F36V} tagged SEM cells. Peaks enriched for H3K27ac are shown in green. (**H**) Correlation of the change in promoter-interaction frequency and the change in H3K27ac (left) and ATAC-seq (right) at MYB-bound MCC peaks, following 24h treatment with dTAG-13 in MYB-FKBP12^{F36V} tagged SEM cells. Spearman correlation coefficients are shown for peaks that show a statistically significant decrease in interaction frequency (FDR <0.05, green) or where interaction frequency is unchanged (gray).

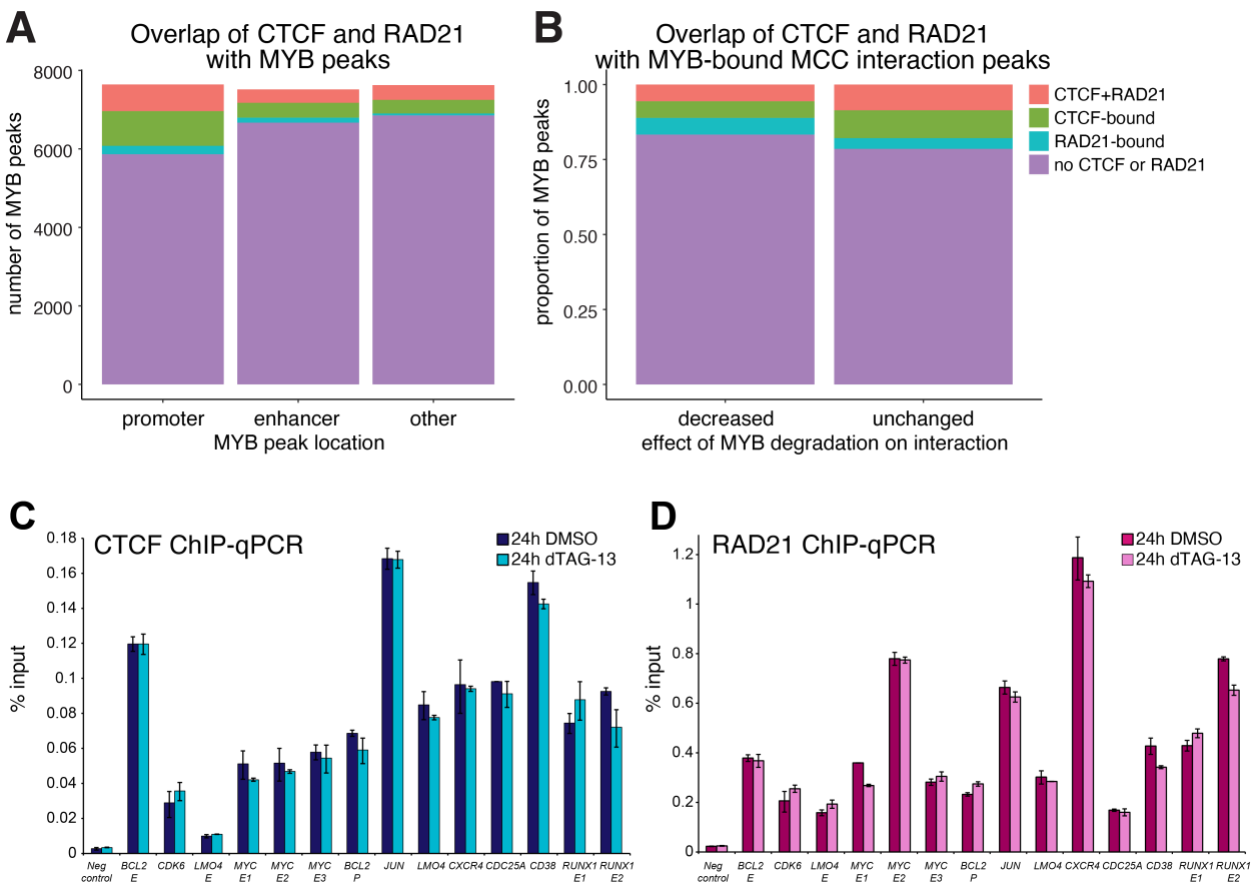

Supplemental Figure 6.
(**A**) Proportion of MYB peaks that overlap with CTCF or RAD21. Peaks are separated based on genomic location. (**B**) Proportion of MYB peaks at MCC interaction sites that overlap with CTCF or RAD21. Peaks are separated based on the effect of dTAG-13 treatment on interaction frequency. ChIP-qPCR for CTCF (**C**) and RAD21 (**D**) in MYB-FKBP12^{F36V} tagged SEM cells following treatment with DMSO or 0.5 μM dTAG-13 for 2h or 24h. Representative of three biological replicates.

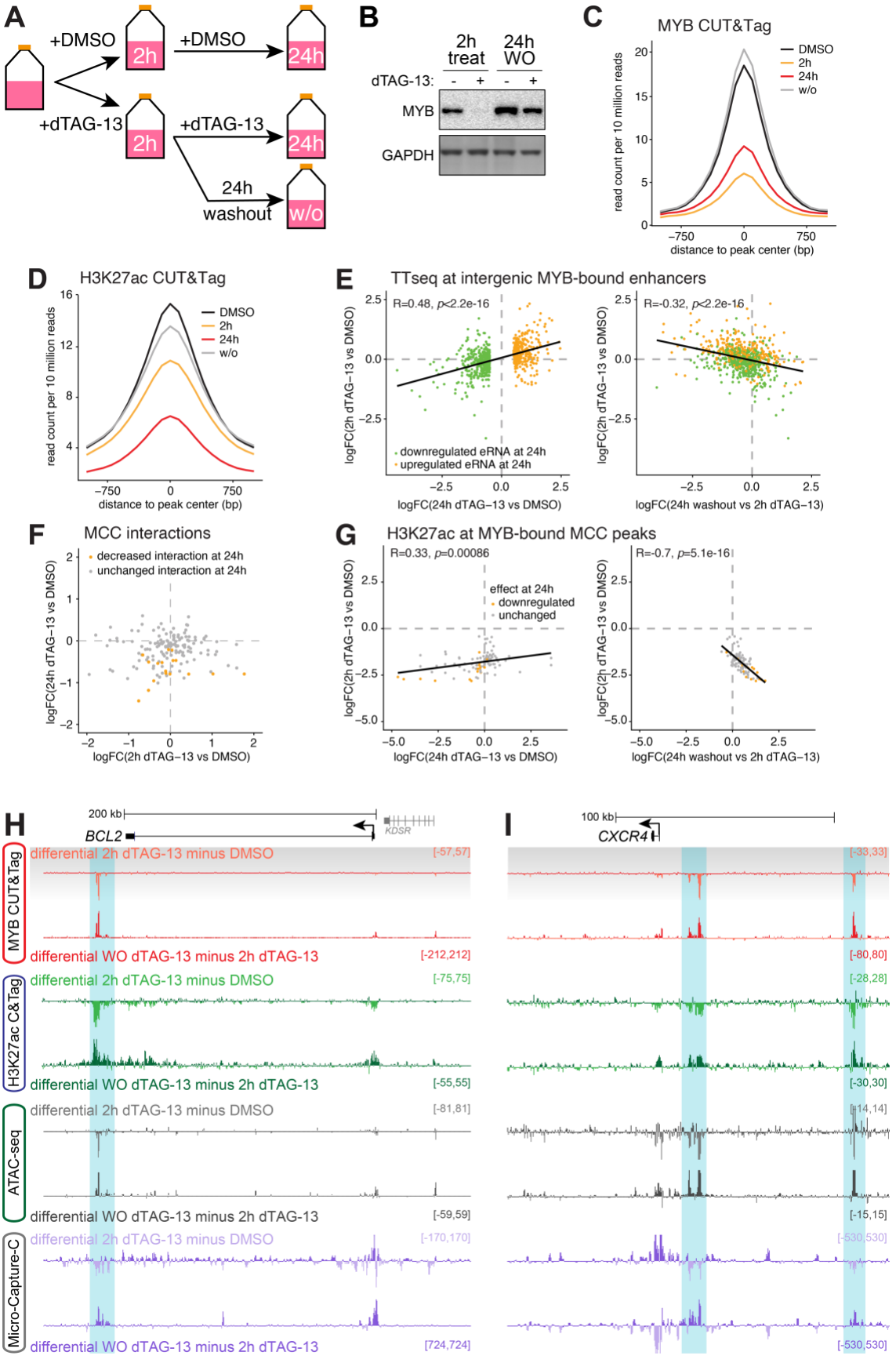
A
+DMSO
2h
+DMSO
24h
+dTAG-13
2h
+dTAG-13
24h
24h
washout
w/o
B
2h
treat
24h
WO
dTAG-13:
- + - +
MYB
GAPDH
C
MYB CUT&Tag
DMSO
2h
24h
w/o
read count per 10 million reads
distance to peak center (bp)
D
H3K27ac CUT&Tag
DMSO
2h
24h
w/o
read count per 10 million reads
distance to peak center (bp)
E
TTseq at intergenic MYB-bound enhancers
R=0.48, p<2.2e-16
R=-0.32, p<2.2e-16
downregulated eRNA at 24h
upregulated eRNA at 24h
logFC(2h dTAG−13 vs DMSO)
logFC(24h dTAG−13 vs DMSO)
logFC(24h washout vs 2h dTAG−13)
F
MCC interactions
decreased interaction at 24h
unchanged interaction at 24h
logFC(24h dTAG−13 vs DMSO)
logFC(2h dTAG−13 vs DMSO)
G
H3K27ac at MYB-bound MCC peaks
R=0.33, p=0.00086
R=-0.7, p=5.1e-16
effect at 24h
downregulated
unchanged
logFC(2h dTAG−13 vs DMSO)
logFC(24h dTAG−13 vs DMSO)
logFC(24h washout vs 2h dTAG−13)
H
200 kb
BCL2
KDSR
MYB CUT&Tag
differential 2h dTAG-13 minus DMSO
[-57,57]
differential WO dTAG-13 minus 2h dTAG-13
[-212,212]
H3K27ac C&Tag
differential 2h dTAG-13 minus DMSO
[-75,75]
differential WO dTAG-13 minus 2h dTAG-13
[-55,55]
ATAC-seq
differential 2h dTAG-13 minus DMSO
[-81,81]
differential WO dTAG-13 minus 2h dTAG-13
[-59,59]
Micro-Capture-C
differential 2h dTAG-13 minus DMSO
[-170,170]
differential WO dTAG-13 minus 2h dTAG-13
[724,724]
I
100 kb
CXCR4
[-33,33]
[-80,80]
[-28,28]
[-30,30]
[-14,14]
[-15,15]
[-530,530]
[-530,530]

Supplemental Figure 7.
(**A**) Schematic showing the timecourse workflow. MYB-FKBP12^{F36V} tagged SEM cells were treated with DMSO or 0.5 μM dTAG-13 for 2h or 24h before processing. After 2h treatment, a second batch of cells were transferred to drug-free medium and allowed to recover for 24h before processing (washout). (**B**) Western blot for MYB in MYB-FKBP12^{F36V} tagged SEM cells treated with DMSO (-) or 0.5 μM dTAG-13 (+) for 2h, or 2h treatment followed by 24h washout in drug-free medium. GAPDH is used as loading control. Representative of three biological replicates. (**C**) Mean MYB CUT&Tag signal at MYB-bound enhancers in control (untreated) MYB-FKBP12^{F36V} tagged SEM cells treated with dTAG-13 for 2h or 24h, or treated for 2h then washed out for 24h (w/o). (**D**) Mean H3K27ac CUT&Tag signal at MYB-bound enhancers in control (untreated), dTAG-13-treated or washout MYB-FKBP12^{F36V} tagged SEM cells. (**E**) Correlation between the change in gene expression measured by TT-seq after 2h and 24h dTAG-13 treatment (left) or after 2h dTAG-13 treatment and subsequent washout (right). Enhancers are coloured by the change at 24h, FDR<0.05. Spearman correlation coefficients are shown. (**F**) Correlation between the change in MCC interaction frequency at MYB-bound peaks after 2h and 24h dTAG-13 treatment. Peaks are coloured by the change at 24h, FDR<0.05. (**G**) Correlation between the change in H3K27ac at MYB-bound MCC peaks after 2h and 24h dTAG-13 treatment (left) or after 2h dTAG-13 treatment and subsequent washout (right). Peaks are coloured by the change in MCC interaction frequency at 24h, FDR<0.05. Spearman correlation coefficients are shown. Micro-Capture-C (MCC), MYB and H3K27ac CUT&Tag and ATAC-seq in MYB-FKBP12^{F36V} tagged SEM cells at *BCL2* (**H**) and *CXCR4* (**I**), under control (untreated), 2h or 24h dTAG-13 treatment, or washout (WO). Differential tracks show the difference in interaction frequency between the indicated conditions.

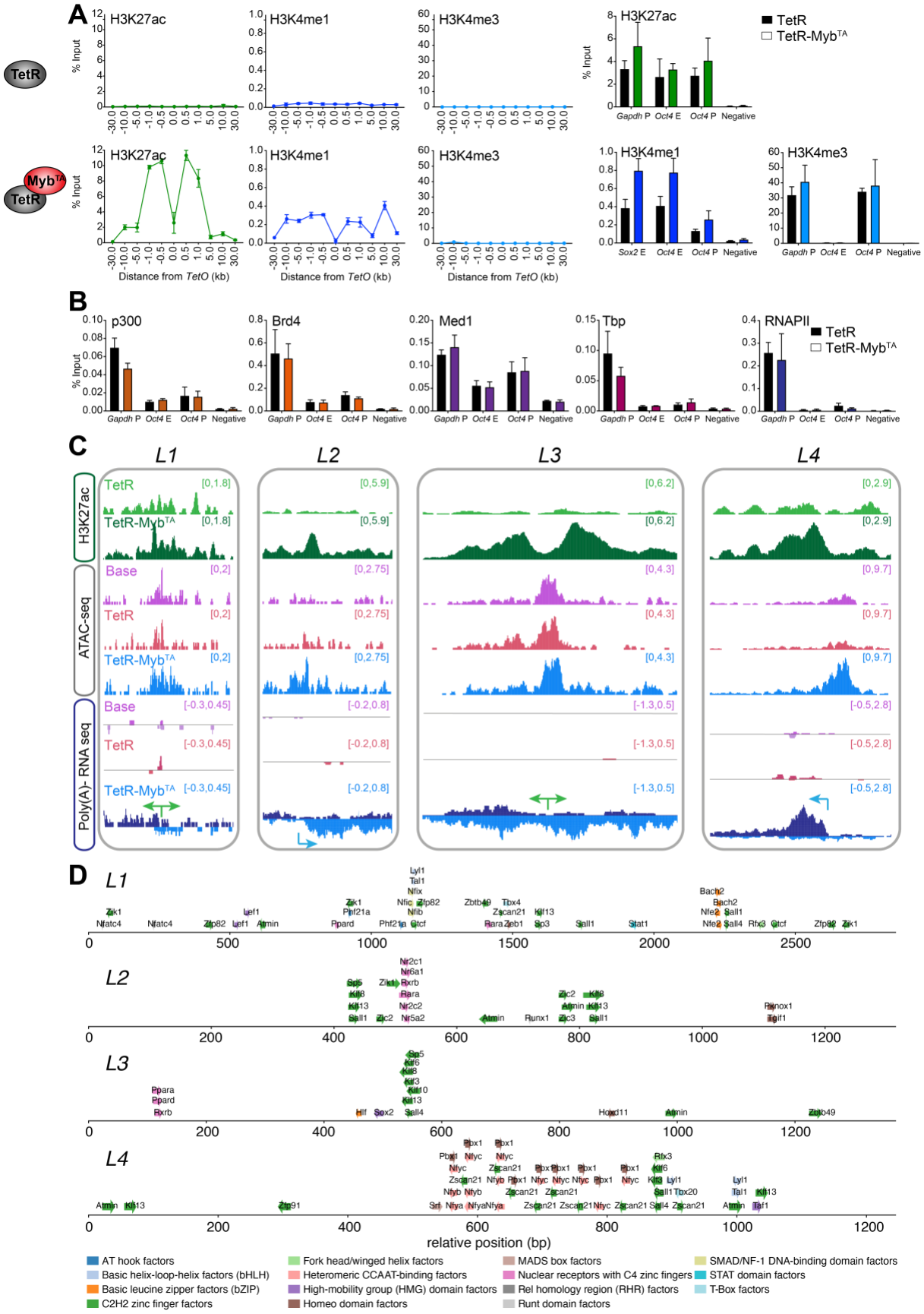
A
TetR
MybTA
TetR
H3K27ac
H3K4me1
H3K4me3
% Input
TetR
TetR-MybTA
Gapdh P
Oct4 E
Oct4 P
Negative
Sox2 E
Distance from TetO (kb)
B
p300
Brd4
Med1
Tbp
RNAPII
C
L1
L2
L3
L4
H3K27ac
ATAC-seq
Poly(A)- RNA seq
Base
D
relative position (bp)
AT hook factors
Basic helix-loop-helix factors (bHLH)
Basic leucine zipper factors (bZIP)
C2H2 zinc finger factors
Fork head/winged helix factors
Heteromeric CCAAT-binding factors
High-mobility group (HMG) domain factors
Homeo domain factors
MADS box factors
Nuclear receptors with C4 zinc fingers
Rel homology region (RHR) factors
Runt domain factors
SMAD/NF-1 DNA-binding domain factors
STAT domain factors
T-Box factors

Supplemental Figure 8.
(**A**) ChIP-qPCR analysis across the *TetO*-containing locus in cell lines stably expressing either TetR (top row) or TetR-Myb^{TA} (bottom row) and at endogenous loci (bottom row), for H3K27ac (left), H3K4me1 (middle) and H3K4me3 (right). Error bars represent the standard deviation from three biological replicates. (**B**) ChIP-qPCR for p300, Brd4, Med1, Tbp, RNAPII at endogenous loci in the indicated TetR mESCs. Error bars represent the standard deviation from three biological replicates. (**C**) H3K27ac ChIP-seq, ATAC-seq and poly-A minus RNA-seq at *L1-4* loci. Arrows represent predominant direction of transcription (green = bidirectional; blue = unidirectional). (**D**) Motif locations within ATAC-seq peak sequences *L1-L4* for expressed TFs, $q < 0.05$. Block arrows denote individual motif occurrences, with arrow direction indicating strand orientation. Arrows are coloured by TF class. Where motifs overlap spatially, they are collapsed by motif and stacked vertically and ranked by a composite score (CPM × $-\log_{10}$(q-value)), with higher-scoring motifs positioned above lower-scoring ones.

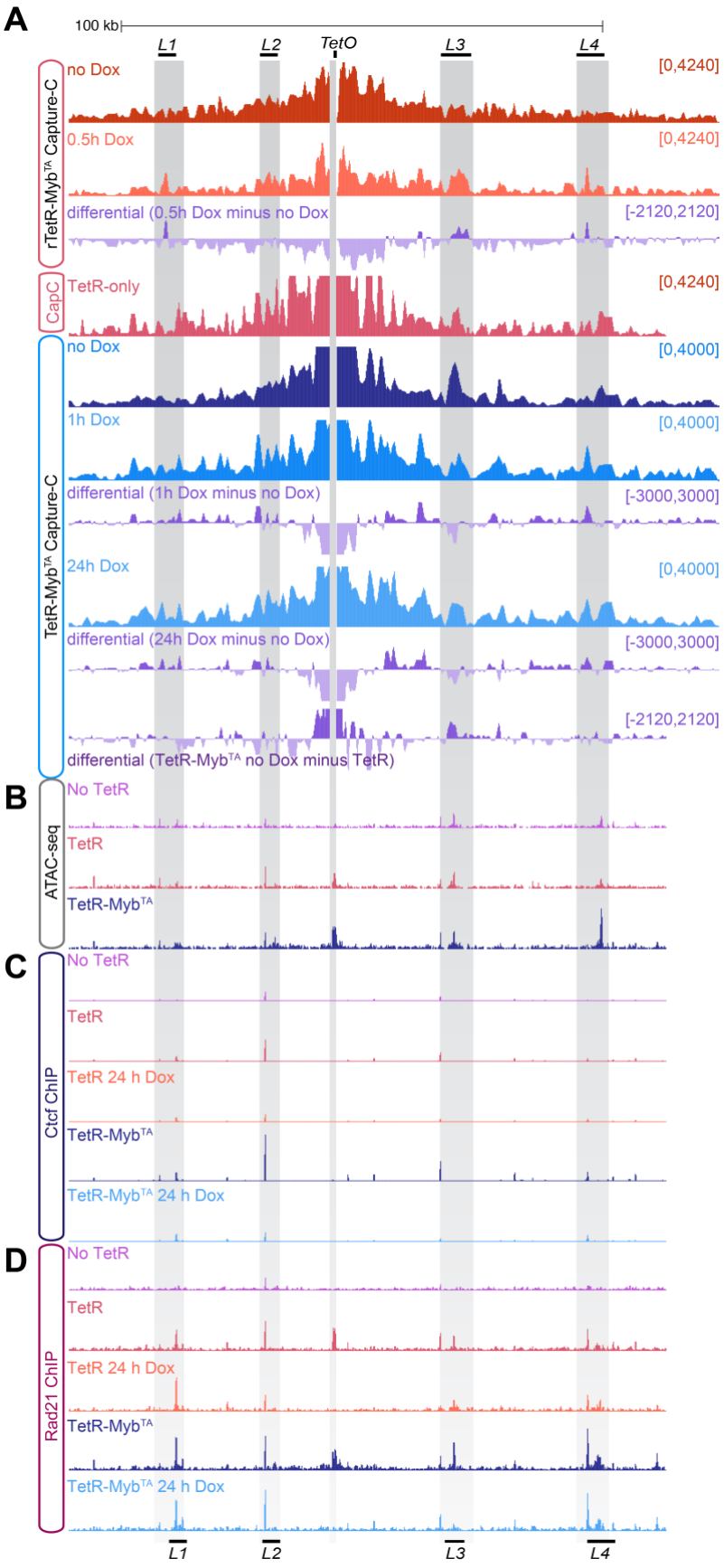
A
100 kb
L1
L2
TetO
L3
L4
rTetR-MybTA Capture-C
no Dox
[0,4240]
0.5h Dox
[0,4240]
differential (0.5h Dox minus no Dox
[-2120,2120]
CapC
TetR-only
[0,4240]
TetR-MybTA Capture-C
no Dox
[0,4000]
1h Dox
[0,4000]
differential (1h Dox minus no Dox)
[-3000,3000]
24h Dox
[0,4000]
differential (24h Dox minus no Dox)
[-3000,3000]
[-2120,2120]
differential (TetR-MybTA no Dox minus TetR)
B
ATAC-seq
No TetR
TetR
TetR-MybTA
C
Ctcf ChIP
No TetR
TetR
TetR 24 h Dox
TetR-MybTA
TetR-MybTA 24 h Dox
D
Rad21 ChIP
No TetR
TetR
TetR 24 h Dox
TetR-MybTA
TetR-MybTA 24 h Dox
L1
L2
L3
L4

Supplemental Figure 9.
(**A**) Capture C across the *TetO* locus in rTetR-Myb^{TA}, TetR-only and TetR-Myb^{TA} expressing cells following treatment with doxycycline. Differential track shows the difference in interaction frequency between untreated and doxycycline conditions, or between untreated TetR-Myb^{TA} and TetR-only cells. (**B**) ATAC-seq in cells not expressing TetR, expressing TetR-only or TetR-Myb^{TA}. ChIP-seq for Ctcf (**C**) or Rad21 (**D**) in cells not expressing TetR, expressing TetR-only or TetR-Myb^{TA}, under control (untreated) conditions or following 24h treatment with doxycycline.

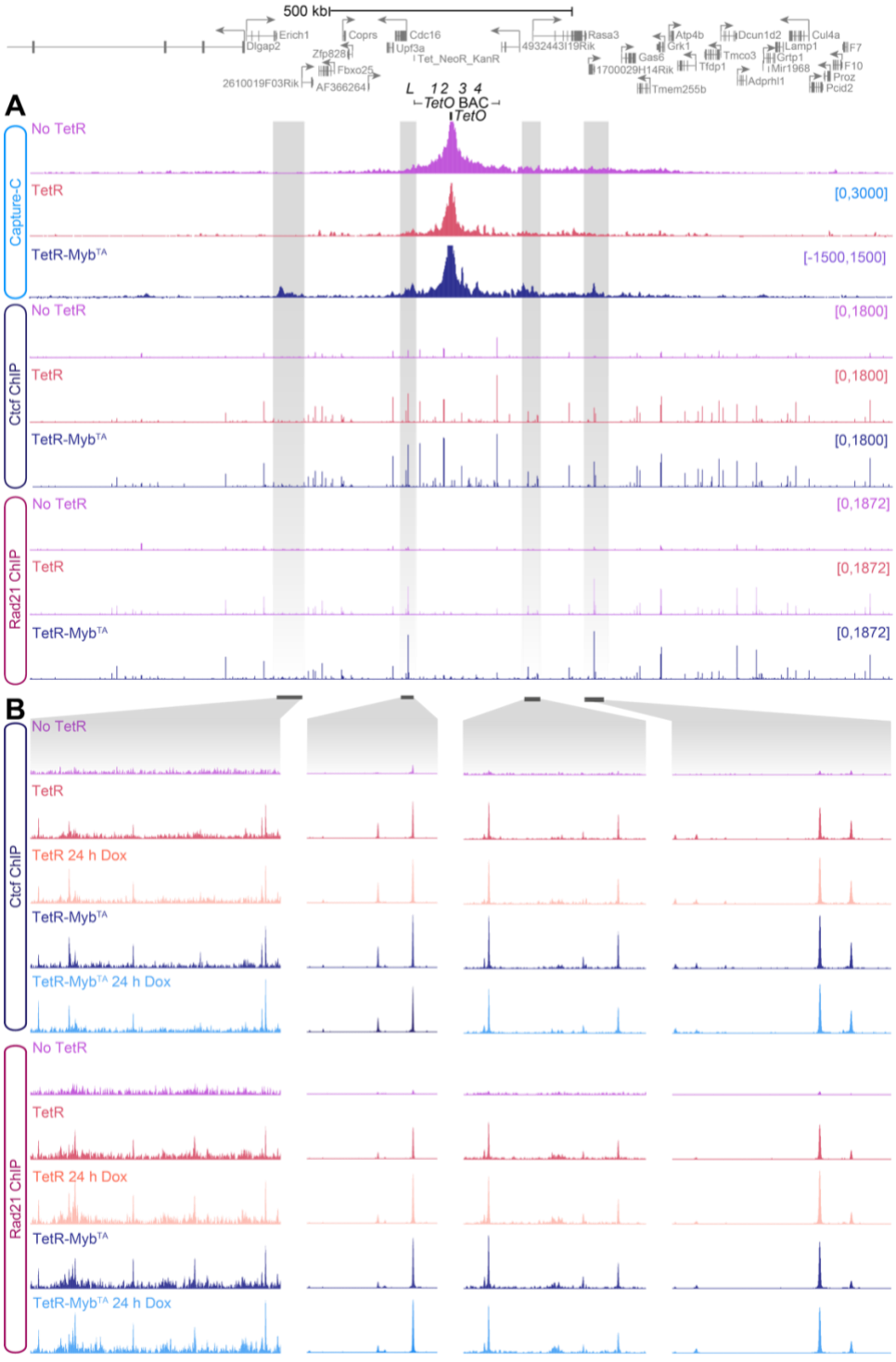

Supplemental Figure 10.
(**A**) Capture C and ChIP-seq for Ctcf and Rad21 across the broad *TetO* locus in cells not expressing TetR, expressing TetR-only or TetR-Myb^{TA} under control (untreated) conditions or following 24h treatment with doxycycline. (**B**) As in A, expanded view of the regions indicated by vertical gray shading.

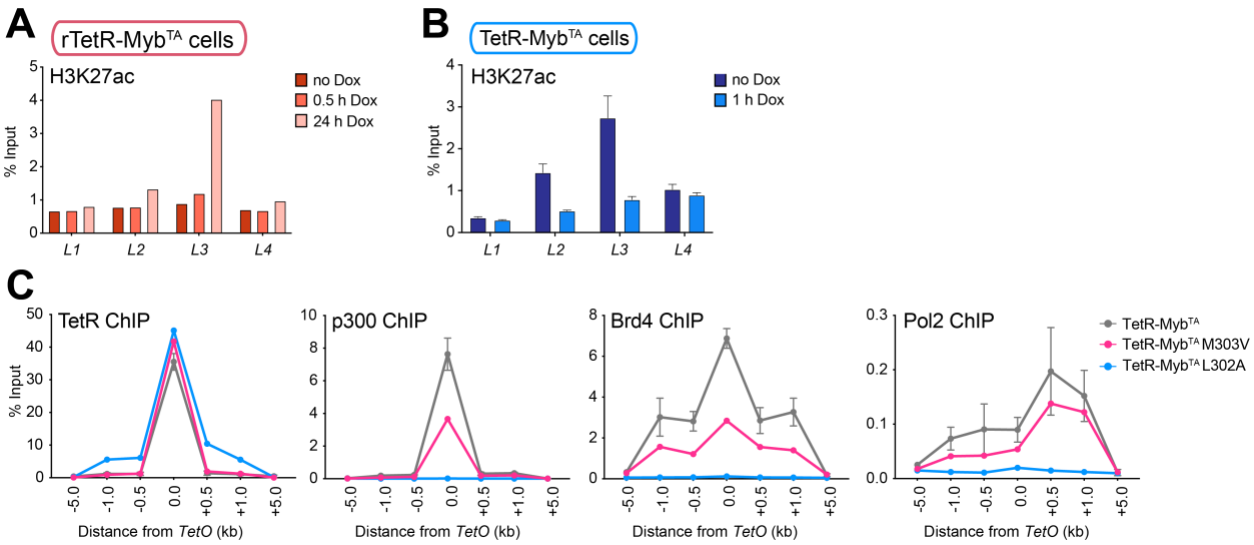

Supplemental Figure 11.
(**A**) ChIP-qPCR for H3K27ac at *L1-4* following doxycycline treatment for 0.5 and 24h in rTetR-Myb^{TA} expressing cells. Representative of three biological replicates. (**B**) As in (A), ChIP-qPCR in TetR-Myb^{TA} expressing cells following doxycycline treatment for 1 h. Error bars represent the standard deviation from three biological replicates. (**C**) ChIP-qPCR analysis across the *TetO* containing locus in cell lines stably expressing either TetR-MYB^{TA} (gray), TetR-Myb^{TA}M303V (pink), or TetR-Myb^{TA}L302A (blue), using antibodies against TetR, p300, Brd4 and RNAPII (Pol2). Error bars represent the standard deviation from three biological replicates.

References

1. Hyle J, Zhang Y, Wright S, et al. Acute depletion of CTCF directly affects MYC regulation through loss of enhancer-promoter looping. *Nucleic Acids Res*. 2019;47(13):6699-6713.
2. Gossen M, Freundlieb S, Bender G, Müller G, Hillen W, Bujard H. Transcriptional Activation by Tetracyclines in Mammalian Cells. *Science*. 1995;268(5218):1766--1769.
3. Martinez N, Drescher B, Riehle H, et al. The oncogenic fusion protein RUNX1-CBFA2T1 supports proliferation and inhibits senescence in t(8;21)-positive leukaemic cells. *BMC Cancer*. 2004;4:44.
4. Godfrey L, Crump NT, Thorne R, et al. DOT1L inhibition reveals a distinct subset of enhancers dependent on H3K79 methylation. *Nature Communications*. 2019;10(1):2803.
5. Kerry J, Godfrey L, Repapi E, et al. MLL-AF4 Spreading Identifies Binding Sites that Are Distinct from Super-Enhancers and that Govern Sensitivity to DOT1L Inhibition in Leukemia. *Cell Reports*. 2017;18(2):482--495.
6. Crump NT, Smith AL, Godfrey L, et al. MLL-AF4 cooperates with PAF1 and FACT to drive high-density enhancer interactions in leukemia. *Nat Commun*. 2023;14(1):5208.
7. Grandi FC, Modi H, Kampman L, Corces MR. Chromatin accessibility profiling by ATAC-seq. *Nat Protoc*. 2022;17(6):1518-1552.
8. Buenrostro JD, Giresi PG, Zaba LC, Chang HY, Greenleaf WJ. Transposition of native chromatin for fast and sensitive epigenomic profiling of open chromatin, DNA-binding proteins and nucleosome position. *Nature Methods*. 2013;10(12):1213--1218.
9. Langmead B, Trapnell C, Pop M, Salzberg SL. Ultrafast and memory-efficient alignment of short DNA sequences to the human genome. *Genome Biol*. 2009;10(3):R25.
10. Li H, Handsaker B, Wysoker A, et al. The Sequence Alignment/Map format and SAMtools. *Bioinformatics*. 2009;25(16):2078-2079.
11. Heinz S, Benner C, Spann N, et al. Simple Combinations of Lineage-Determining Transcription Factors Prime cis-Regulatory Elements Required for Macrophage and B Cell Identities. *Molecular Cell*. 2010;38(4):576--589.
12. Zhang Y, Liu T, Meyer CA, et al. Model-based analysis of ChIP-Seq (MACS). *Genome Biol*. 2008;9(9):R137.
13. Kent WJ, Sugnet CW, Furey TS, et al. The human genome browser at UCSC. *Genome Res*. 2002;12(6):996-1006.
14. Ramírez F, Ryan DP, Grüning B, et al. deepTools2: a next generation web server for deep-sequencing data analysis. *Nucleic Acids Research*. 2016;44(W1):W160--W165.
15. Grant CE, Bailey TL, Noble WS. FIMO: scanning for occurrences of a given motif. *Bioinformatics*. 2011;27(7):1017-1018.
16. Vorontsov IE, Eliseeva IA, Zinkevich A, et al. HOCOMOCO in 2024: a rebuild of the curated collection of binding models for human and mouse transcription factors. *Nucleic Acids Res*. 2024;52(D1):D154-D163.
17. Kolberg L, Raudvere U, Kuzmin I, Vilo J, Peterson H. gprofiler2 -- an R package for gene list functional enrichment analysis and namespace conversion toolset g:Profiler. *F1000Res*. 2020;9.
18. Schwalb B, Michel M, Zacher B, et al. TT-seq maps the human transient transcriptome. *Science*. 2016;352(6290):1225--1228.

19. Kim D, Paggi JM, Park C, Bennett C, Salzberg SL. Graph-based genome alignment and genotyping with HISAT2 and HISAT-genotype. *Nat Biotechnol*. 2019;37(8):907-915.
20. Liao Y, Smyth GK, Shi W. featureCounts: an efficient general purpose program for assigning sequence reads to genomic features. *Bioinformatics*. 2014;30(7):923--930.
21. Chen Y, Chen L, Lun ATL, Baldoni PL, Smyth GK. edgeR v4: powerful differential analysis of sequencing data with expanded functionality and improved support for small counts and larger datasets. *Nucleic Acids Res*. 2025;53(2).
22. Downes DJ, Smith AL, Karpinska MA, et al. Capture-C: a modular and flexible approach for high-resolution chromosome conformation capture. *Nat Protoc*. 2022;17(2):445-475.
23. Davies JOJ, Telenius JM, McGowan SJ, et al. Multiplexed analysis of chromosome conformation at vastly improved sensitivity. *Nature Methods*. 2016;13(1):74--80.
24. Hamley JC, Li H, Denny N, Downes D, Davies JOJ. Determining chromatin architecture with Micro Capture-C. *Nat Protoc*. 2023;18(6):1687-1711.
25. Hua P, Badat M, Hanssen LLP, et al. Defining genome architecture at base-pair resolution. *Nature*. 2021;595(7865):125--129.
26. Hentges LD, Sergeant MJ, Cole CB, Downes DJ, Hughes JR, Taylor S. LanceOtron: a deep learning peak caller for genome sequencing experiments. *Bioinformatics*. 2022;38(18):4255-4263.
27. Hao F, Zhang Y, Hou J, Zhao B. Chromatin remodeling and cancer: the critical influence of the SWI/SNF complex. *Epigenetics Chromatin*. 2025;18(1):22.
28. Pratcorona M, Abbas S, Sanders MA, et al. Acquired mutations in ASXL1 in acute myeloid leukemia: prevalence and prognostic value. *Haematologica*. 2012;97(3):388-392.
29. Salomoni P, Perrotti D, Martinez R, Franceschi C, Calabretta B. Resistance to apoptosis in CTLL-2 cells constitutively expressing c-Myb is associated with induction of BCL-2 expression and Myb-dependent regulation of bcl-2 promoter activity. *Proc Natl Acad Sci U S A*. 1997;94(7):3296-3301.
30. Ma T, Chen Y, Yi ZG, et al. BET in hematologic tumors: Immunity, pathogenesis, clinical trials and drug combinations. *Genes Dis*. 2023;10(6):2306-2319.
31. Zhong X, Ma H. Targeting CD38 for acute leukemia. *Front Oncol*. 2022;12:1007783.
32. Cancilla D, Rettig MP, DiPersio JF. Targeting CXCR4 in AML and ALL. *Front Oncol*. 2020;10:1672.
33. Yang L, Rau R, Goodell MA. DNMT3A in haematological malignancies. *Nat Rev Cancer*. 2015;15(3):152-165.
34. Daver N, Venugopal S, Ravandi F. FLT3 mutated acute myeloid leukemia: 2021 treatment algorithm. *Blood Cancer J*. 2021;11(5):104.
35. DiNardo CD, Ravandi F, Agresta S, et al. Characteristics, clinical outcome, and prognostic significance of IDH mutations in AML. *Am J Hematol*. 2015;90(8):732-736.
36. Feng L, Zhang H, Liu T. Multifaceted roles of IKZF1 gene, perspectives from bench to bedside. *Front Oncol*. 2024;14:1383419.
37. Cante-Barrett K, Pieters R, Meijerink JP. Myocyte enhancer factor 2C in hematopoiesis and leukemia. *Oncogene*. 2014;33(4):403-410.
38. Zhang P, Lu R. The Molecular and Biological Function of MEF2D in Leukemia. *Adv Exp Med Biol*. 2024;1459:379-403.
39. Delgado MD, Leon J. Myc roles in hematopoiesis and leukemia. *Genes Cancer*. 2010;1(6):605-616.

40. Godfrey L, Crump NT, O'Byrne S, et al. H3K79me2/3 controls enhancer-promoter interactions and activation of the pan-cancer stem cell marker PROM1/CD133 in MLL-AF4 leukemia cells. *Leukemia*. 2021;35(1):90-106.
41. Wilkinson Adam C, Ballabio E, Geng H, et al. RUNX1 Is a Key Target in t(4;11) Leukemias that Contributes to Gene Activation through an AF4-MLL Complex Interaction. *Cell Reports*. 2013;3(1):116--127.
42. Owen C, Fitzgibbon J, Paschka P. The clinical relevance of Wilms Tumour 1 (WT1) gene mutations in acute leukaemia. *Hematol Oncol*. 2010;28(1):13-19.